Spring 2004

The Extent of the White Chuck Tuff, a High Temperature Pyroclastic Flow Deposit, Glacier Peak, Washington

Gerald T. Ladd

Western Washington University, jerrytladd@gmail.com

Follow this and additional works at: https://cedar.wwu.edu/wwuet

Part of the Geology Commons

THE EXTENT OF THE WHITE CHUCK TUFF,
A HIGH TEMPERATURE PYROCLASTIC FLOW DEPOSIT,
GLACIER PEAK, WASHINGTON

by

Gerald T. Ladd

Accepted in Partial Completion

Of the Requirements for the Degree

Master of Science

Moheb A. Ghali, Dean of the Graduate School

ADVISORY COMMITTEE
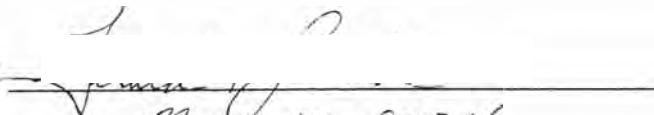
Chair, Dr. _____
Dr. Scott Babcock

Dr. _____
Dr. Russ Burmester

Dr. _____
Dr. Bernard Housen

MASTER'S THESIS

In presenting this thesis in partial fulfillment of the requirements for a master's degree at Western Washington University, I agree that the Library shall make its copies freely available for inspections. I further agree that the copying of this thesis in whole or in part is allowable only for scholarly purposes. It is understood, however, that any copying or publication of this thesis project for commercial purposes, or for financial gain, shall not be allowed without my written permission.

Signature _____

Date _____ May 16, 2004 _____

MASTER'S THESIS

In presenting this thesis in partial fulfillment of the requirements for a master's degree at Western Washington University, I grant to Western Washington University the non-exclusive royalty-free right to archive, reproduce, distribute, and display the thesis in any and all forms, including electronic format, via any digital library mechanisms maintained by WWU.

Gerald T. Ladd
jerrytladd@gmail.com
March 9, 2018

The Extent of the White Chuck Tuff,
A High Temperature Pyroclastic Flow Deposit,
Glacier Peak, Washington

A Thesis
Presented to
The Faculty of
Western Washington University

In Partial Fulfillment
Of the requirements for the Degree
Master of Science

By
Gerald T. Ladd
May 2004

Abstract

The White Chuck Tuff, a massive deposit approximately 15 m thick, caps two terraces in the White Chuck River valley covering an area of approximately 5 km^2 at the base of Glacier Peak, Washington. Three major post-glacial eruption cycles from Glacier Peak reportedly occurred approximately from 12,000 to 11,250 years ago (White Chuck Assemblage), from 5,500 to 5,100 years ago (Kennedy Creek Assemblage), and from 1,800 to 250 years ago (recent eruptions). West of Glacier Peak, pyroclastic and lahar deposits from all three episodes are found in drainages out to Puget Sound 100 km away. The White Chuck Tuff has been assumed to be approximately 11, 500 years old (Beget, 1981) and not found west of Camp Creek in the White Chuck River Valley, approximately 17 km from Glacier Peak. Anisotropy of magnetic susceptibility, paleomagnetic, petrographic, and geochemical procedures were conducted to characterize the tuff deposit. Similar laboratory procedures were conducted on five distal pyroclastic deposits to determine if they were unconsolidated runout of the White Chuck Tuff.

Flow direction, paleomagnetic directions and paleomagnetic poles, mineralogy, and chemical composition of the proximal indurated White Chuck Tuff indicate that it was emplaced as a single unit at temperatures exceeding 580° C. The overall flow direction during emplacement was northwesterly down the White Chuck River Valley. The paleomagnetic directions, mineral and chemical compositions are similar amongst the seven sampling sites.

Five distal deposits WC-1, SR-1, SR-2, SR-3, and ST-1 were products of cold to warm (from 22°C to 375°C) debris flows that made their way down the White Chuck

iv

River Valley into the Sauk and North Fork Stillaguamish River Valleys. The paleomagnetic directions amongst the distal deposits were not well defined. The anisotropy of magnetic susceptibility of these deposits had no preferred orientation of the magnetic fabric indicating that the flow direction and individual clast anisotropy were independent of emplacement mechanisms. A viscous magnetization was measured in many of the pumiceous clasts sampled at all of the cooler distal sites and upward directions were measured in the low unblocking temperature range of 100 to 300° C in many of the samples from these sites. The clasts from these deposits had a previous magnetic history before they came to rest at their present location. The chemistry and mineralogy of all five distal sites is similar and indicate dacitic composition.

The virtual geomagnetic pole of distal deposit WC-1 closely corresponds with the 9180 +290/-200 virtual geomagnetic pole of Hagstrum and Champion (2002), which post dates the White Chuck Assemblage. Virtual geomagnetic poles of other distal deposits are not well enough defined to be useful. From field relationships associated with the deposition and location of other deposits (Dravovich et al, 2003), the Glacier Peak distal deposits were probably produced during the Kennedy Creek Assemblage eruption cycle.

The virtual geomagnetic pole of the White Chuck Tuff deposit matches the 12,750 b.p. virtual geomagnetic pole of Hagstrum and Champion (2002). This virtual geomagnetic pole dates the tuff's deposition before the White Chuck Assemblage eruptive cycle. Therfore the previously assumed age of 11,500 b.p. is probably incorrect.

ACKNOWLEDGMENTS

TABLE OF CONTENTS

LIST OF FIGURES

LIST OF TABLES

Introduction

Correlation of ash flow deposits is important in complex volcanic fields because such deposits may provide clues to the regional stratigraphic framework. The White Chuck Tuff, a product of Glacier Peak Volcano (Figure 1a), is such a deposit. The tuff is a massive ash flow deposit believed to cap the White Chuck Assemblage, first named by Tabor and Crowder (1969) for the volcanic deposits resulting from the Late-Pleistocene eruptive episode of Glacier Peak, has and assumed age of approximately 11,500 years b.p.

Late-Pleistocene pyroclastic and lahar deposits contemporaneous with tephra eruptions (G through B) occurred in river drainages surrounding Glacier Peak (Beget, 1981). The Late-Pleistocene eruptions produced pumiceous pyroclastic flows that extended as far as 20 km down valleys. Lahars and alluvium consisting entirely of reworked pyroclastic debris were deposited contemporaneously in the Sauk and North Fork Stillaguamish Valleys as far as 100 km downstream (Beget, 1983). Holocene eruptions had similar eruptive sequences depositing pyroclastic flows and lahars to the west and east of Glacier Peak. Lahars deposited during the Holocene have also been identified to reach Puget Sound.

The purpose of this study is to show the relationship between the White Chuck Tuff deposit in the upper White Chuck River Valley and five possibly correlative distal lahar deposits of the Sauk and North Fork Stillaguamish River Valleys using paleomagnetic, petrographic, and geochemical methods. The principal goals of this study are to determine the (1) depositional relationship between the White Chuck Tuff and the

distal deposits, (2) mode of emplacement of the White Chuck Tuff and distal deposits, and (3) relative emplacement temperature of the deposits.

Previous geologic studies west of Glacier Peak include Vance (1957), Beget (1981) and Dragovich et al (2000). The authors of these studies concluded that during the Late-Pleistocene, deposition of voluminous pyroclastics and lahars caused major drainage changes. An estimated 10 km^3 of volcanic debris, deposited where the city of Darrington is located today, diverted the original western course of the Sauk River into the North Fork Stillaguamish River, to its present route north, into the Skagit River (Figure 1b). Beget (1981) reported that most deposits in this area, approximately 30 km from Glacier Peak, were emplaced during Late Pleistocene volcanic episodes. Dragovich et al (2000) noted that volcanic deposits in the Sauk River and North Fork Stillaguamish River confluence are intercalated with alluvium and glacial outwash. This suggests that there were two separate volcanic episodes younger than 5,000 years ago. If the volcanic debris beneath Darrington was deposited during the Holocene, the Sauk River could have been flowing westward down the North Fork Stillaguamish River only 5,500 years ago (Dragovich, personal communication, 2001).

Petrologic studies of Glacier Peak deposits have been performed by Ford (1957), Tabor and Crowder (1969) and most recently by Taylor (2001). The earliest studies concluded that Glacier Peak is a dacitic stratovolcano with isolated mafic volcanic centers distributed between 5 and 10 km south of Glacier Peak. Taylor (2001) focused on the petrology and geochemistry of four Late Pleistocene to Early Holocene mafic vents between 5 and 10 km south of Glacier Peak. Glacier Peak dacite samples were a critical part of Taylor's analysis. Characteristics of the two most evolved mafic centers suggest

2

parent magma mixing with more felsic crustal compositions, similar to evolved Glacier Peak dacites.

A major uncertainty is the age and extent of the White Chuck Tuff, a high volume pyroclastic flow, thought to have been deposited in the upper White Chuck River Valley approximately $11,420 \pm 150$ years ago (Beget 1981, W-4616, p. 46). The dated log, on which this age is based, was located approximately 30 km west of the tuff deposit in an outcrop near the mouth of the White Chuck River. The date was interpreted as a lower limit to the White Chuck Tuff by Beget (1981) because the stratigraphy at that site had a pumiceous deposit bounded by a lower lahar deposit containing the log, and an upper lahar deposit with rip-up clasts of the White Chuck Tuff. The pumiceous deposit was interpreted as possible distal runout of the White Chuck Tuff.

This tuff deposit has not been identified down stream of Camp Creek in the White Chuck Valley (Tabor and Crowder, 1969), but material from this could have extended farther downstream where it was deposited as unconsolidated laharic fill, such as that of the Sauk/Stillaguamish River divide. The distal deposits were examined in the four areas shown on Figure 1b. Distal deposits that have similar paleomagnetic, mineralogical and chemical characteristics may be contemporaneous with the eruptive event of the White Chuck Tuff.

Figure 1a. The location of the research field area in relation to Glacier Peak, Washington
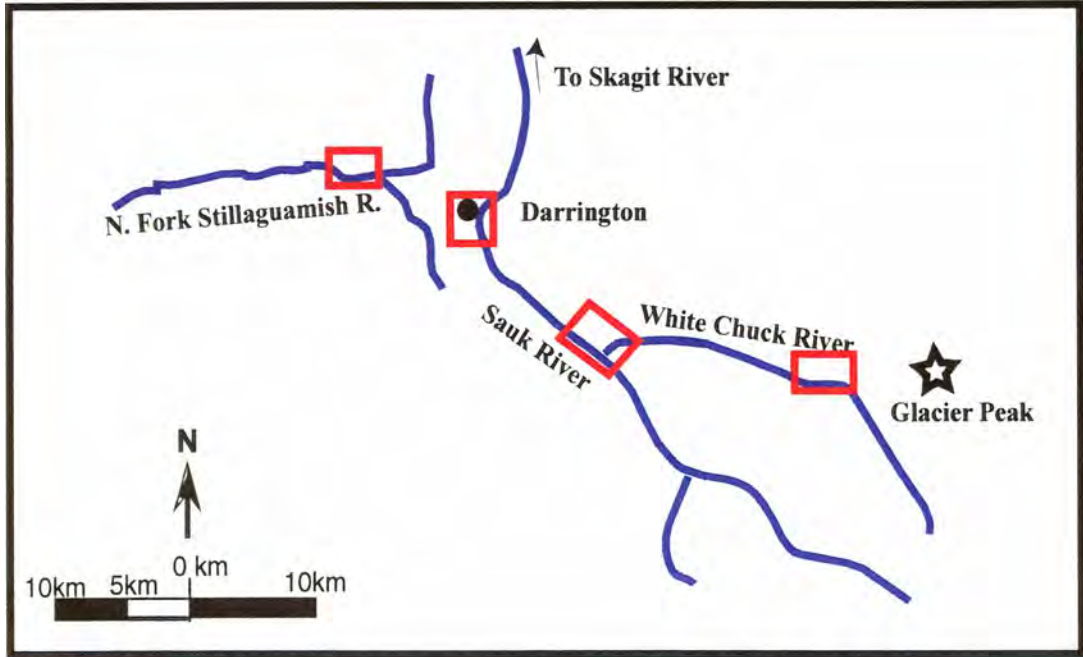
Figure 1b. An enlarged view of the field area showing the location of the four focus study areas west of Glacier Peak.

Glacier Peak

The following discussion describes the major landforms and the geologic makeup of Glacier Peak so that the reader can better evaluate the conclusions regarding correlation of the White Chuck Tuff and distal deposits. The discussion is primarily taken from Vance (1957), Tabor and Crowder (1969), Beget (1981, 1983), Beget et al (1990), Dragovich et al (2000), and Waitt et al (1995).

Regional Setting

Glacier Peak is one of five dormant stratovolcanoes in Washington State (Figure 1a). The Cascade Volcanic Arc is made up of approximately 15 Quaternary stratovolcanoes paralleling the length of the Cascadia Subduction zone where the North American Plate is converging (N50°E) with the Juan de Fuca Plate approximately 45 mm per year (Riddihough, 1984). Glacier Peak is located about 100 km northeast of Seattle, Washington and rises 3,213 m above sea level. There is no evidence that Glacier Peak is older than 700 Ka because all deposits sampled on the flanks of the volcano have normal polarity magnetization (Tabor and Crowder, 1969).

Post-Glacial Eruptive History

Glacier Peak (Figure 2) has had three major eruptive episodes since the retreat of continental glaciers in Western North America. The three episodes produced volcanic

5

Figure 2. The west side of Glacier Peak with the Kennedy (left) and Scimitar (right) glaciers in view.

sequences identified as 1) the White Chuck Assemblage ≈12,000-11,250 years before present (b.p.), 2) the Kennedy Creek Assemblage ≈5,500-5,100 years b.p., and 3) recent eruptions ≈1,800-250 years b.p. (Beget, 1981). Post-glacial eruptions have produced pyroclastic flows, lahars, tephra, and dacite lava. Glacier Peak post-glacial eruptions are second only to Mount St. Helens, in southwest Washington, as the largest and most explosive eruptions in Washington State. To the west, the Late-Pleistocene and Holocene Glacier Peak volcanic episodes filled the White Chuck, Sauk, and North Fork Stillaguamish Rivers with pyroclastic and lahar deposits. A select number of flows reached the Puget Sound over 100 kilometers away from Glacier Peak via the North Fork Stillaguamish and Skagit Rivers (Dragovich et al., 2000).

White Chuck Assemblage: The White Chuck Assemblage is known for its tephra deposits that are used as stratigraphic markers throughout eastern Washington, Idaho, Montana, and Southern parts of Alberta, Canada (Porter, 1978; Westgate and Evans, 1978). These Late-Pleistocene eruptions produced tephra, pyroclastics, and lahars that were deposited on all flanks of the volcano. Pyroclastic and lahar deposits contemporaneous with these tephra eruptions occur in river drainages that originate on Glacier Peak and extend down valleys as far as 20 km (Figure 3a). Lahars and alluvium consisting of reworked pyroclastics were deposited contemporaneously in the Sauk and Stillaguamish Valleys as far as 100 km downstream (Beget, 1983) (Figure 3b). Vance (1957) and Beget (1981) concluded that during this eruptive cycle, a thick sedimentary fan of lahars and volcanic alluvium was deposited in the upper Stillaguamish River Valley diverting the Sauk River north into the Skagit River drainage.

7

Kennedy Creek Assemblage: The eruptions forming the Kennedy Creek Assemblage began about 5,500 years ago (Beget, 1981). The assemblage consists of pyroclastic flow deposits, and non-cohesive and cohesive lahar deposits, which were produced by several eruptive events probably over a period of about 400 years. These deposits extend 135 km down valley from Glacier Peak to near La Conner in the Puget Lowland (Dragovich et al., 2000). Terraces of Kennedy Creek Assemblage deposits are found in the White Chuck, Sauk, and Skagit River Valleys. The total estimated volume of the preserved Kennedy Creek Assemblage from the flanks of Glacier Peak to the Puget Sound is estimated to be 2-3 km^3 (Beget, 1981).

Recent Eruptions: The last major eruptions occurred from 1,800 to 250 years ago (Beget, 1981) that produced small tephra eruptioins, pyroclastics, and lahars. Most lahars and pyroclastic flows traveled down the Suiattle River into the Sauk River about 30 km from the volcano. Lahars also traveled as far as 15 km down the White Chuck River Valley.

Figure 3a. Unsorted pyroclastic deposits of the (Beget 1982) in the White Chuck River
Valley approxmately 10 km west of Glacier Peak.

Figure 3b. Lahar deposits in the North Fork Stillaguamish River flood plain approximately
50 km west of Glacier Peak.

Description of Deposits

White Chuck Tuff

A15 m thick, cliff-forming, tuff deposit (Figure 4) caps a terrace paralleling the White Chuck River Valley from Glacier Creek to Camp Creek about 17 km from Glacier Peak (Figure 5a and b). Described in detail by Tabor and Crowder (1969) and Beget (1981), the indurated tuff has well-developed columnar jointing that generally extends from the top to the bottom of the deposit (Figure 6). A thin zone at the base of the tuff deposit, ranging from 10 cm to a meter thick, is less well indurated and lacks jointing (Figure 6). This friable zone typically forms a re-entrant under the indurated tuff. There are no indications that separate flow events formed this deposit. The tuff is massive and pumice lapilli are observed to be concentrated in the upper part of the flow with the lithic dacite clasts concentrated near the base. Mafic crystals in the tuff are primarily hornblende, orthopyroxene, clinopyroxene, with minor amounts of biotite (Beget, 1981). The deposit is not welded, but is locally indurated from settling pressures and heat. The texture of the tuff is seen in Figure 7, which is a photo taken from the Western Washington University scanning electron microscope (SEM). The glass shards appear to be altered and the individual particles are not welded together. The deposit does not show fiamme structure due to pumice collapse, which indicates that the pumice fragments were not hot enough to be ductile.

Approximately 15 km from Glacier Peak, the upper 1-2 m of the deposit are pink to pinkish-red. This discoloration is interpreted as a hydrothermally altered zone

diagnostic of a high temperature emplacement that probably formed when the White

Chuck Tuff was cooling (Crandell, 1980).

Figure 4. View south looking up from the White Chuck River Trail of the cliff-forming White Chuck Tuff. Note the prismatic jointing near the top.
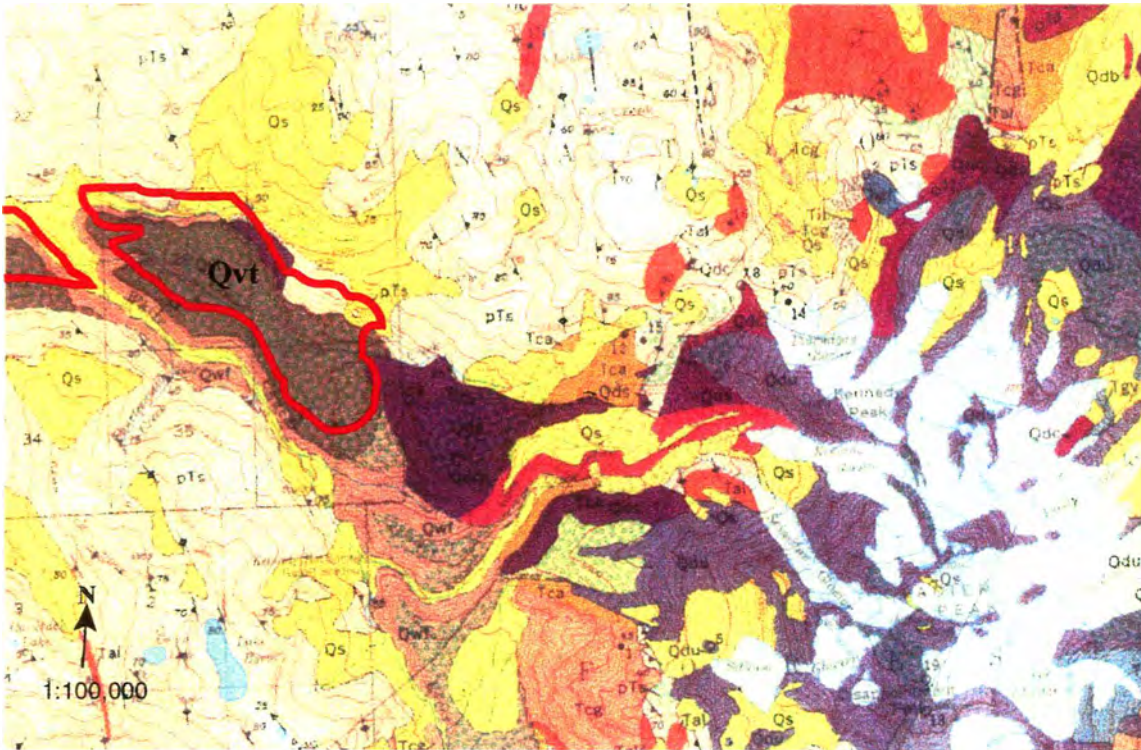
Figure 5a. Geologic map of the west flank of Glacier Peak. The White Chuck Tuff is mapped in dark brown as Qvt, outlined in red (Tabor and Crowder, 1969).

Figure 5b. View east from the base of Glacier Peak down the White Chuck River Valley. The White Chuck Tuff creates the prominent terraces down the center of the White Chuck River Valley.

13
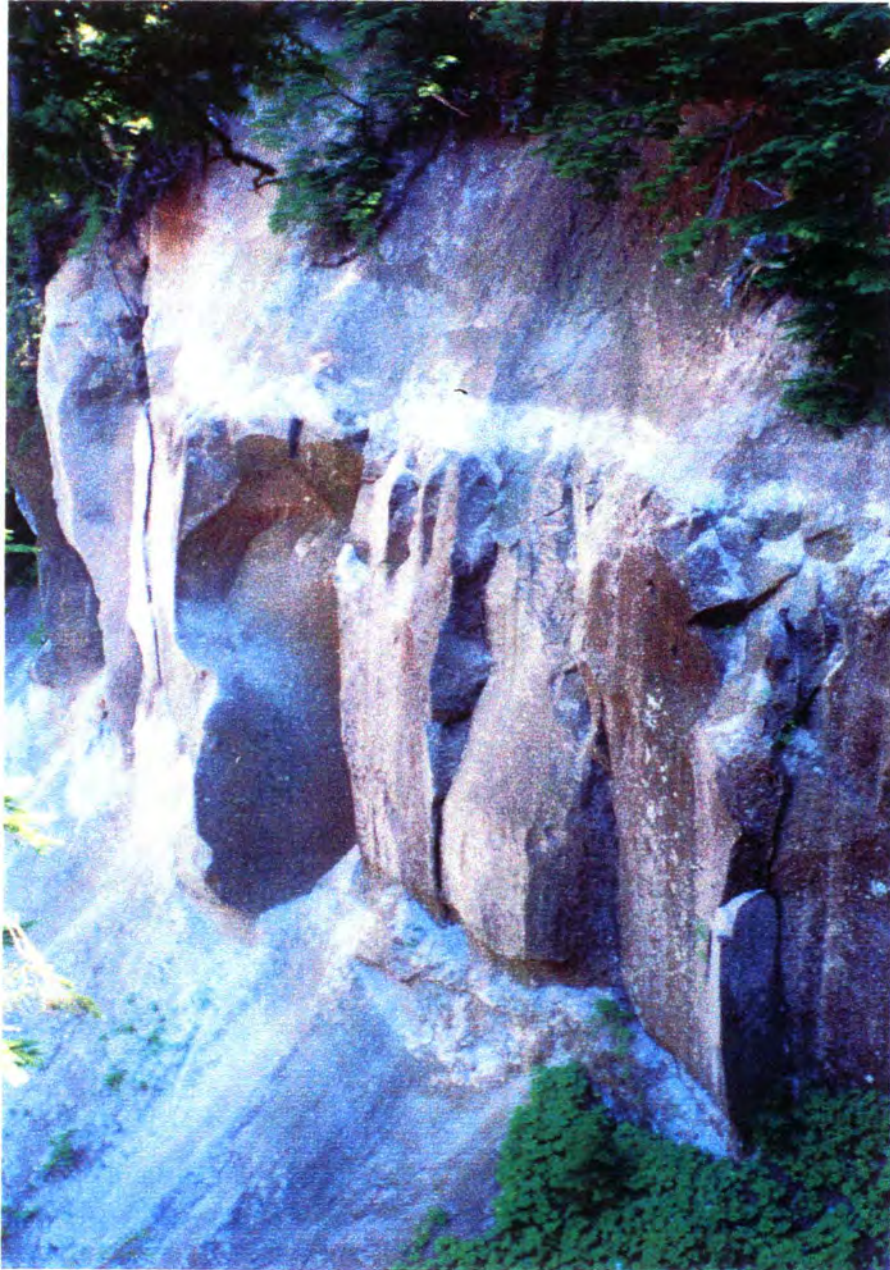
Figure 6. A view of the White Chuck Tuff in its entire section about 15 m thick.
This outcrop is a landslide scarp in the Fire Creek valley. The base,
about 30 cm thick, is a moderately friable zone which lacks jointing.
The major portion of the deposit has columnar jointing. Above the jointing
at the top of the deposit are later pumiceous deposits.

14
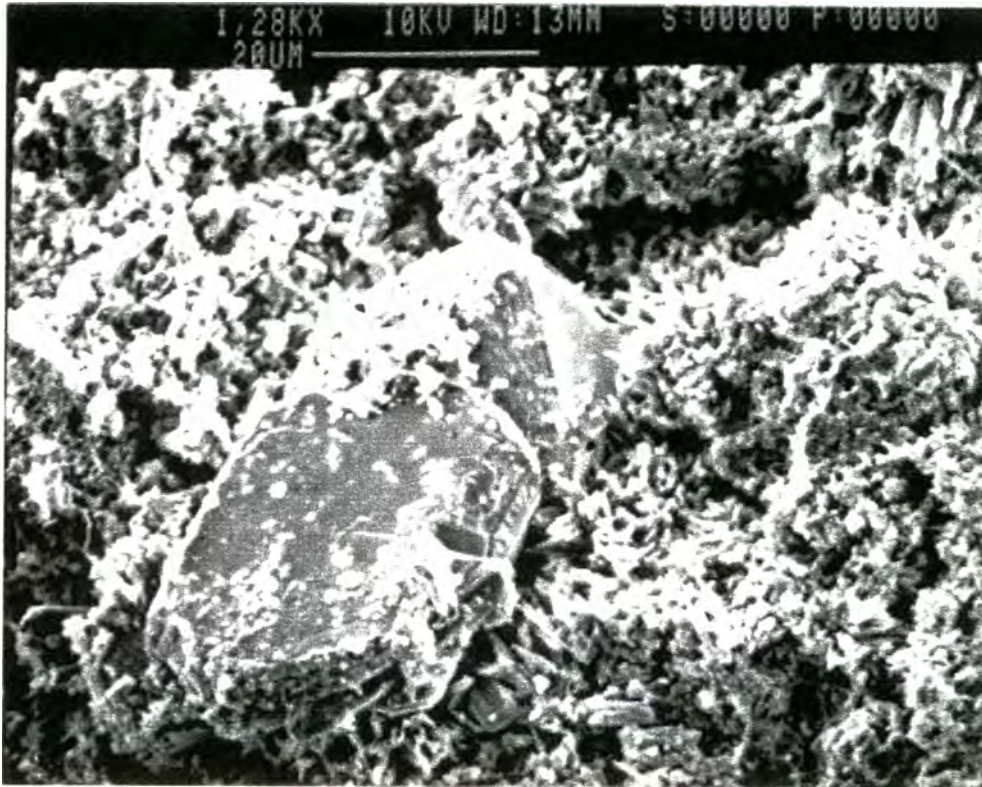
Figure 7. A photo micrograph of the White Chuck Tuff. The ~20 micrometer mineral grain in view is surrounded by a vesicular groundmass. This example shows that the groundmass is not glassy, but made up of spongy clay particles resulting from devitrification of the glass.

The age of the tuff has been identified by dating a log in a lahar deposit near

mouth of the White Chuck River, near the distal deposits, that appears to be conformably

below lahar deposits that contain tuff fragments. The log is about 11,500 years old and

Beget suggests that because the deposit does not contain tuff fragments that the White

Chuck Tuff was probably produced about this same time, as well as tephra layer B,

11,250 b.p. It is not known how far west of Camp Creek the tuff originally extended, but

large blocks of the tuff occur farther downstream in reworked parts of the White Chuck

Assemblage and are also found in the distal deposits in the White Chuck River and Sauk

River (Beget, 1981).

Distal Deposits

The distal deposits studied in this project are believed to be of Late-Pleistocene

age based on stratigraphic position (Beget, 1981). Many deposits of the same lithologies

occur along the river valleys out to the Puget Sound. The most distal deposit sampled for

this project is approximately 50 km from Glacier Peak in the North Fork Stillaguamish

River bank about 2 km east of Darrington. Deposits further than 50 km are less

consolidated and are deemed to be of laharic origin. The more consolidated deposits

were sampled because of the possibility that heat might have played an important part in

their formation and they may also represent distal deposits of the White Chuck Tuff.

Distal deposits, defined in this study as being >30 km west of Glacier Peak, are

pumiceous lahar deposits exposed in creek beds, river valleys, and road cuts. These

deposits are ≤3 m thick consist largely of pumice and dacite clasts suspended in a dacite-

16

rich, sandy groundmass (Figure 8). The deposits are unconsolidated, but compacted enough to form steep-sided banks along rivers and creeks (Figure 9a, b). The compaction is most likely due to settlement of fine and coarse particles during deposition.

Flow boundaries are visible between deposits, but the ages of the individual flows are not easily determined. This is interpreted to be due to the lack of vegetation in the valleys at the time of peak eruptive cycles, and little material suitable for ^{14}C dating has been located (Dragovich et al., 2000). The distal deposits may be correlative with either the White Chuck Assemblage or the Kennedy Creek Assemblage (Dragovich, personal communication, 2001).

The suspended clasts are light gray nonvesicular dacite and more vesicular dacite. Pumice clasts are also present and sometimes reversely graded. Cross-beds seen at the top of the North Fork Stillaguamish site have concentrations of pumice clasts in each cross-bed (Figure 10). Most pumice clasts are rounded and up to 50 cm in diameter. Figure 11 shows a tephra layer that was deposited as a thin consolidated lens between the more massive laharic deposits.
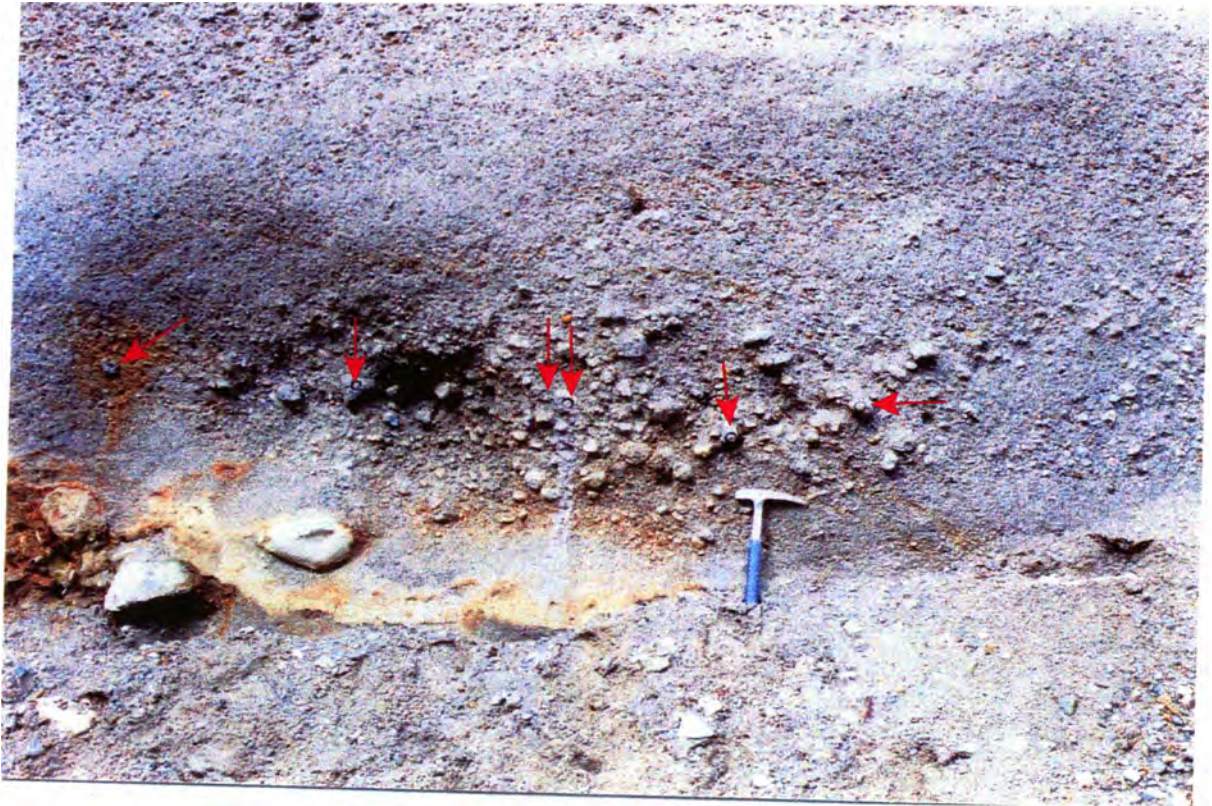
Figure 8. Distal deposit (SR-1), which is typical of the distal deposits containing vesicular and non-vesicular clasts suspended in a fine grained sandy matrix. Core samples of pumiceous dacite clasts were taken from the locations shown by the red arrows.

Figure 9a. A view of distal deposit (ST-1) along the North Fork Stillaguamish River. The deposit is consolidated enough to form steep river banks, but it is easily eroded.
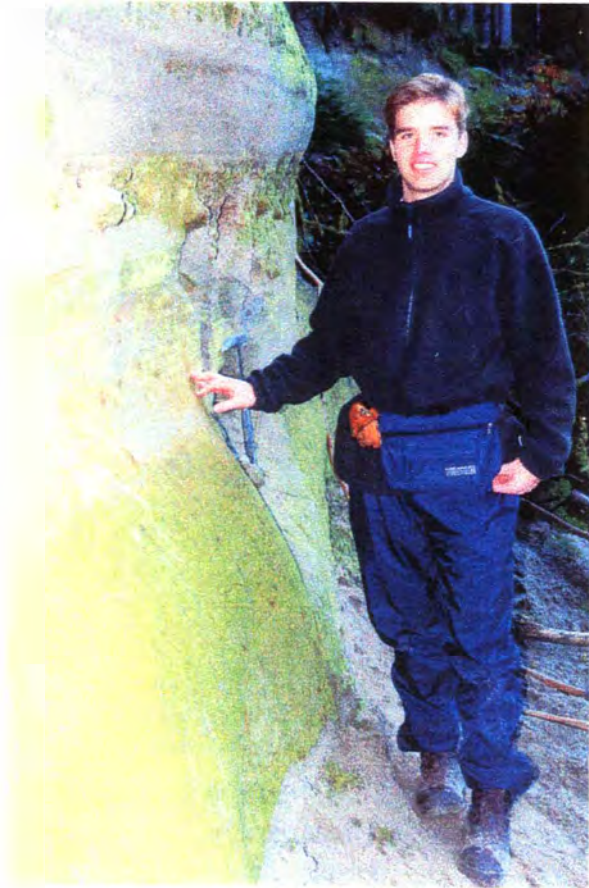
Figure 9b. A close up view of the distal deposit in figure 9a, showing the steep sides of the deposit, fine grained matrix, and dacite clasts. These clasts occur at approximately the height of the author's shoulder.

Figure 10. Cross beds at the top of distal deposit ST-1 that have reversely graded gray sandy graundmass and orange-yellow weathered pumice.

Figure 11. A prominant tephra layer separating two lahar deposits. The tephra layer is approxmately 6 cm thick and is not as easily eroded as the unconsolidated lahar deposits.

Methodology of Study

Field Study and Sampling

A reconnaissance survey of the White Chuck Tuff and distal deposits was conducted over a period of several months. The White Chuck Tuff, in the upper White Chuck River Valley, and five down stream locations in the Sauk River and North Fork Stillaguamish River Valleys (Figure 12 and 13) were chosen for this study because of good exposure and potential for proximal and distal tuff deposit correlation. At each of twelve sample sites the rock unit was described and samples were collected for laboratory analyses.

Individually oriented core samples of the indurated White Chuck Tuff and lithic clasts of the unconsolidated distal deposits were used for magnetic susceptibility, paleomagnetic, petrographic, and chemical evaluation. A sampling scheme was arranged to accommodate paleomagnetic studies in the two distinct locations. Seven sample sites were selected to adequately cover the White Chuck Tuff laterally and stratigraphically (Figure 12). Twenty oriented drill cores were collected from the face of the outcrop at each sampling location. Sample collection started from bottom left and ended at top right (Figure 14). Each site was sampled using a cordless electric drill to drive a 2.5 cm inside diameter diamond drill bit. Orientations of the core samples were obtained using a Brunton pocket transit and core orienter. Field descriptions of the outcrop were also made at each site (Appendix I).

Five downstream sample locations were chosen to assess the relationship between the distal deposits of unconsolidated pumiceous lahars and the White Chuck Tuff (Figure

21

14). A minimum of five oriented samples were collected from each distal deposit location. Clasts >20 cm were drilled and collected using the same method as used for the White Chuck Tuff. Smaller clasts tended to get dislodged while drilled in place. These clasts were oriented in the field and drilled in the lab. All cores were cut into specimens 2.2 cm long.

Most drill cores were longer than the 2.2 cm, which yielded samples that were useful for petrographic and chemical anaylsis. The cylindrical specimens were ideal for thin sections on 7.5x2.5 cm glass slides and each specimen yielded approximately 20 g of material for chemical analysis.
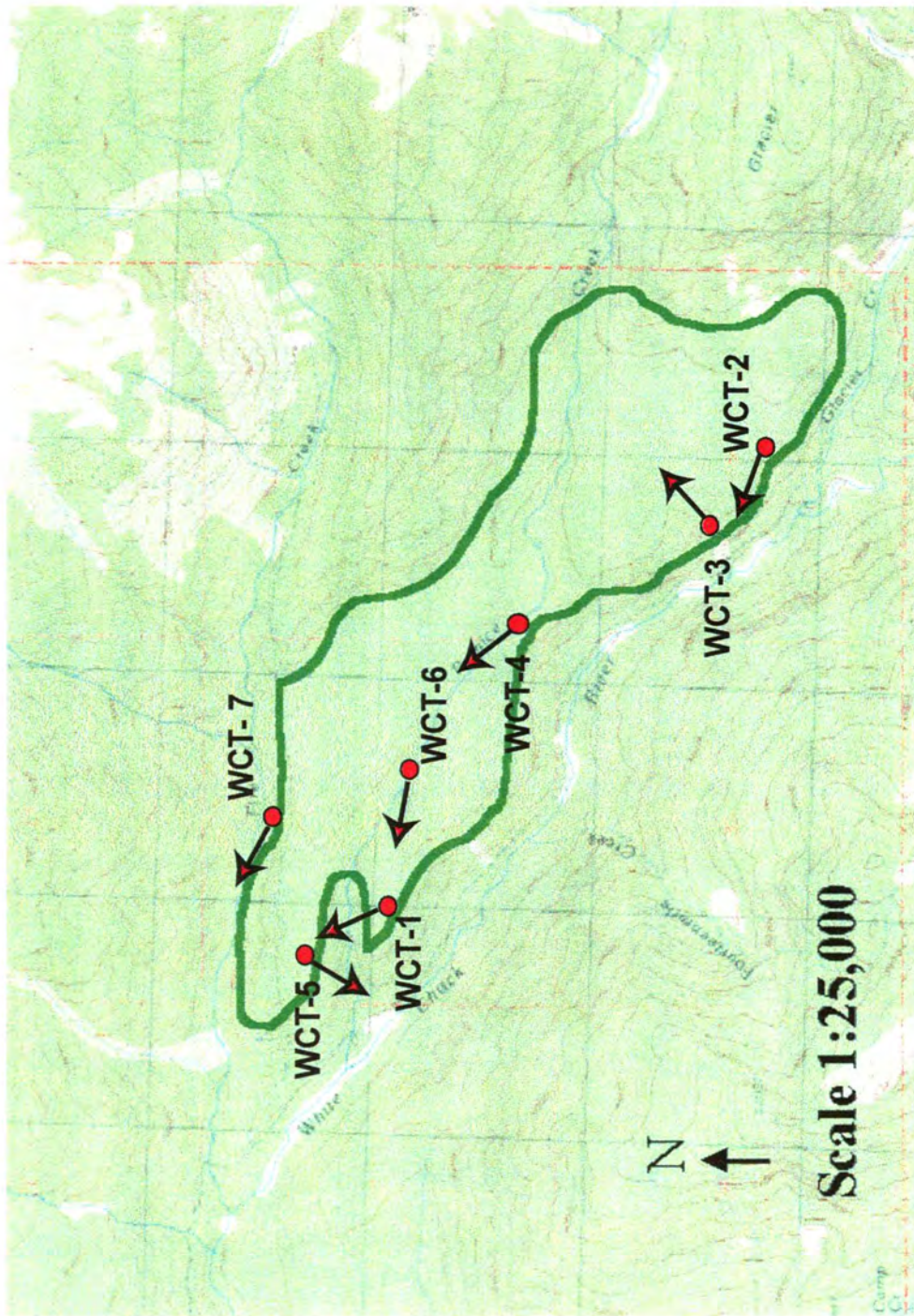
Figure 12. Distribution of the White Chuck Tuff deposit in the upper White Chuck River Valley. Seven localities were sampled covering the deposit both laterally and stratigraphically. The arrows indicate the flow direction at each site extrapolated from Anisotropy of Magnetic Susceptibility data.
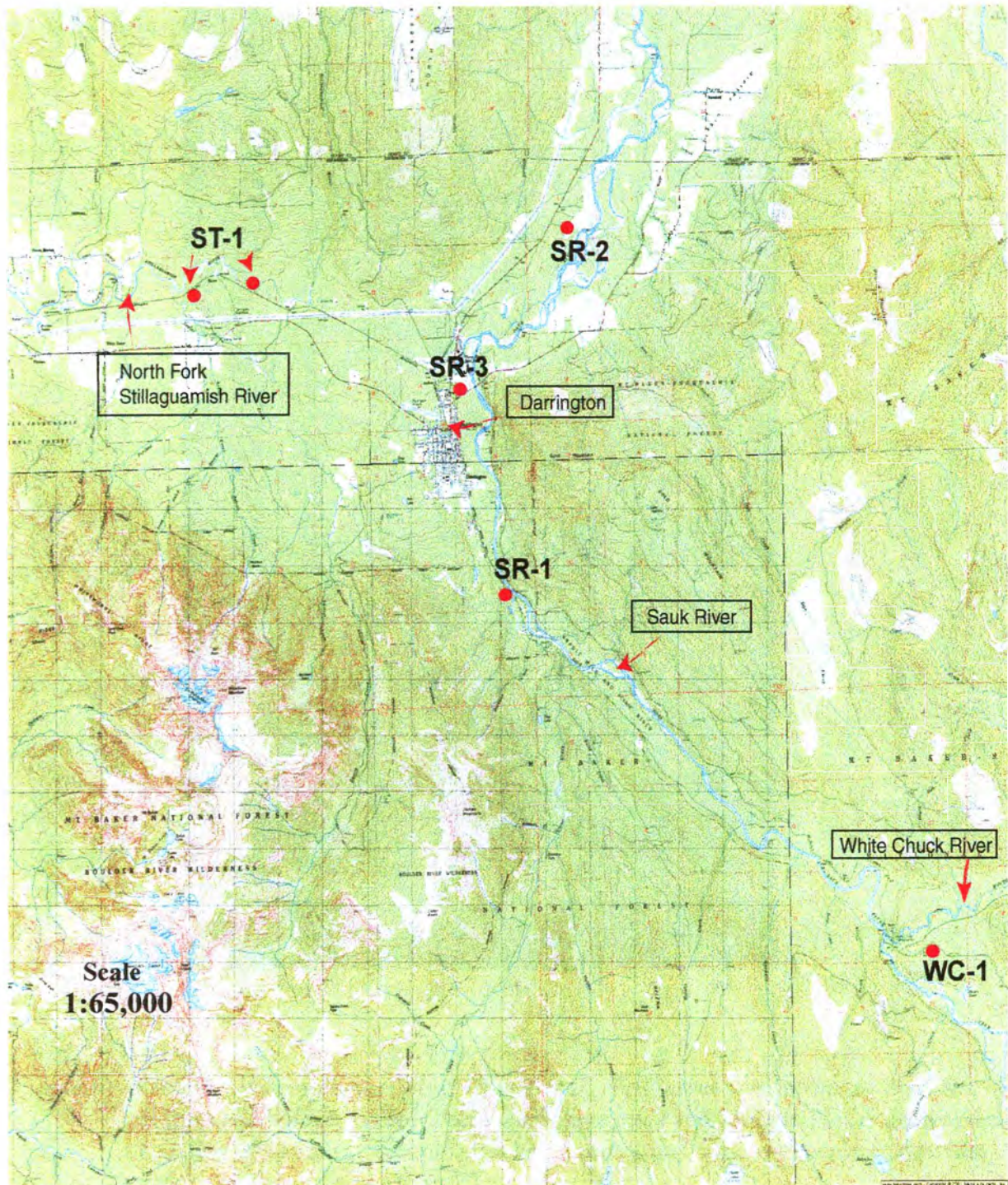
Figure 13. Distal deposit sample locations in the White Chuck, Sauk, and North Fork Stillaguamish River Valleys.
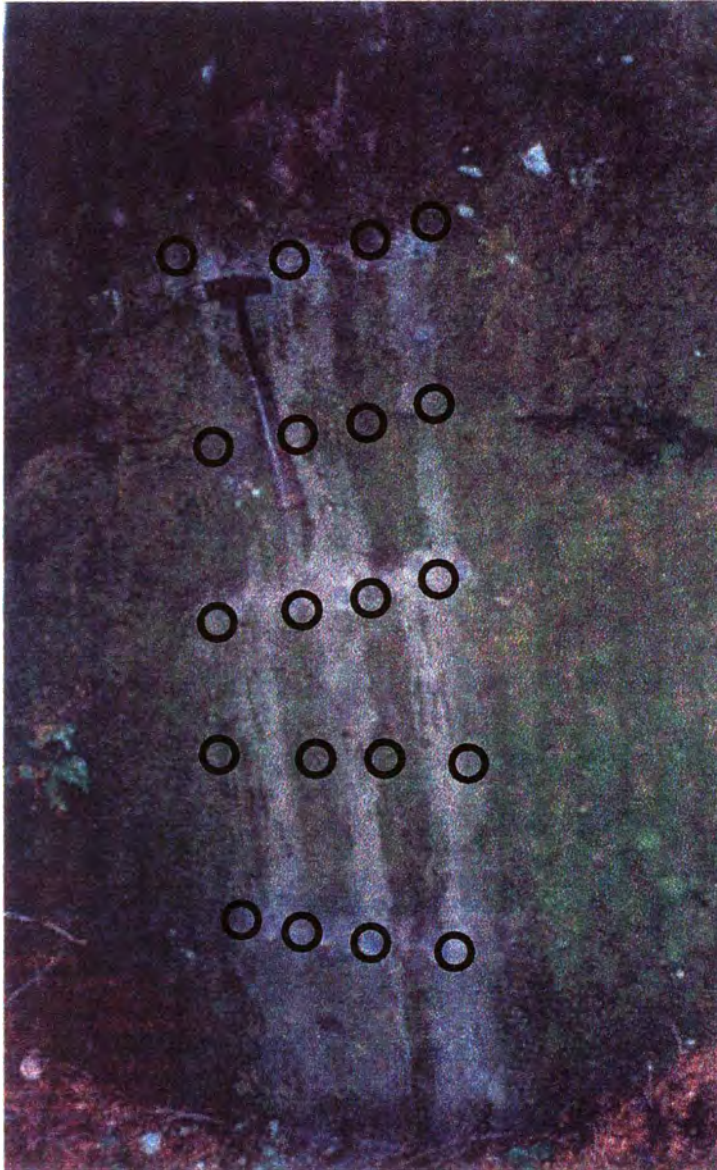
Figure 14. Sampling scheme in the White Chuck Tuff. Drill cores were collected from left to right and bottom to top. There were three rows and four samples in each row equaling 20 samples. Sample sites had corners, walls and overhangs to provide a variety of orientations for added randomness.

Magnetic Studies

Paleomagnetism: Paleomagnetism is primarily the study of the ancient geomagnetic field recorded by rocks. Igneous rocks acquire a magnetic direction parallel to the Earth's magnetic field at the time they cooled below the Curie temperature of their magnetic minerals. In detail, the range of temperatures over which igneous rocks record the ambient geomagnetic field depends on the rate of cooling, mineral compositions, and grain sizes. The properties of common magnetic minerals in igneous rocks are referenced from Dunlop and Ozdemir (1997). To characterize the remanence of these rocks, the natural remanent magnetization (NRM) was progressively thermally demagnetized. The unblocking temperature of components of magnetization that are identified can be used to infer emplacement temperatures, if the composition of the magnetic minerals is well constrained. In order to discriminate between an emplacement at ambient temperature and an emplacement at a temperature significantly above the ambient temperature, a paleomagnetic study was carried out using the method developed by Hoblitt and Kellogg (1979).

The NRM of the proximal, indurated White Chuck Tuff and related distal unconsolidated deposits might indicate spatial evolution of a high temperature pyroclastic flow. Three signatures of NRM at the time of deposition are possible when analyzing individual clasts within volcanic debris deposits (Hoblitt and Kellogg, 1979). In Type I deposits all clasts are above their maximum blocking temperature when deposited and would have acquired their total NRMs parallel to the geomagnetic field. The measured directions will be closely grouped about the field direction that was present during cooling (Figure 15a). Type II deposits occur if all the clasts are magnetized elsewhere,

26

transported, then deposited below their lowest blocking temperature. The total NRM would have been acquired prior to deposition and the measured remanent directions would be randomly scattered due to rotation during transport (Figure 15b). Type III deposits are intermediate between Type I and II; all clasts are deposited below their maximum blocking temperatures, but above the temperature of their minimum blocking temperature. The demagnetization path of clasts from a Type III deposit would contain two partial NRM components, high unblocking temperature and low unblocking temperature components (Figure 15c). The high-temperature component is acquired prior to deposition and thus will be in random directions, whereas the low-temperature component is acquired after the clasts came to rest and will be parallel to the direction of the geomagnetic field that was present during cooling. Deposition is not the only mechanism by which a type II deposit could be partially remagnetized and appears like a type III deposit. Among these mechanisms are viscous remagnetization, reheating partial thermal magnetization and chemical or crystallization remagnetization.

The NRM was measured with a 2-G Enterprises Model 755 Superconducting Rock Magnetometer. To determine components of magnetization the samples were thermally demagnetized using an ASC TD-48 thermal demagnetizer. Demagnetization was accomplished by subjecting the samples to a certain temperature in a shielded oven for 20 minutes, and then cooling them in a zero field with forced air for 10 minutes. The magnetization of the samples was then measured in the magnetometer. Once the samples were measured the process was repeated at successively higher temperatures until the samples were demagnetized. The White Chuck Tuff samples were demagnetized in temperature steps of 50° C until 600° C. The distal deposit samples were demagnetized

in temperature steps of 25° C until 400° C and then 50° C temperature steps until 600° C. The smaller temperature step for the lower temperature range of the distal deposit samples was used to constrain the laboratory unblocking temperature of the low temperature component to within 25° C. Specimens were pretreated prior to being thermally demagnetized using low temperature demagnetization.

Low temperature demagnetization (LTD) is an effective method of removing soft (low coercivity) components of remanence in magnetite-bearing specimens by passing the magnetite through its low-temperature transition (~120 K). Once the specimen is below the critical temperature the specimens are brought back to room temperature and measured. The distal deposit samples underwent this method of "magnetic cleaning" prior to thermal demagnetization. Approximately 10% of the NRM were erased by the LTD method. This was important to remove the soft components that were most likely related to viscous remagnetization.

A variety of rock magnetic methods including Isothermal Remanent Magnetization (IRM), thermal demagnetization of IRM (Lowrie, 1990), Viscous Remanent Magnetization (VRM) tests, and thermo-magnetic curves were used to constrain magnetic mineralogy. (See Appendix II, Rock magnetic methods, for details)
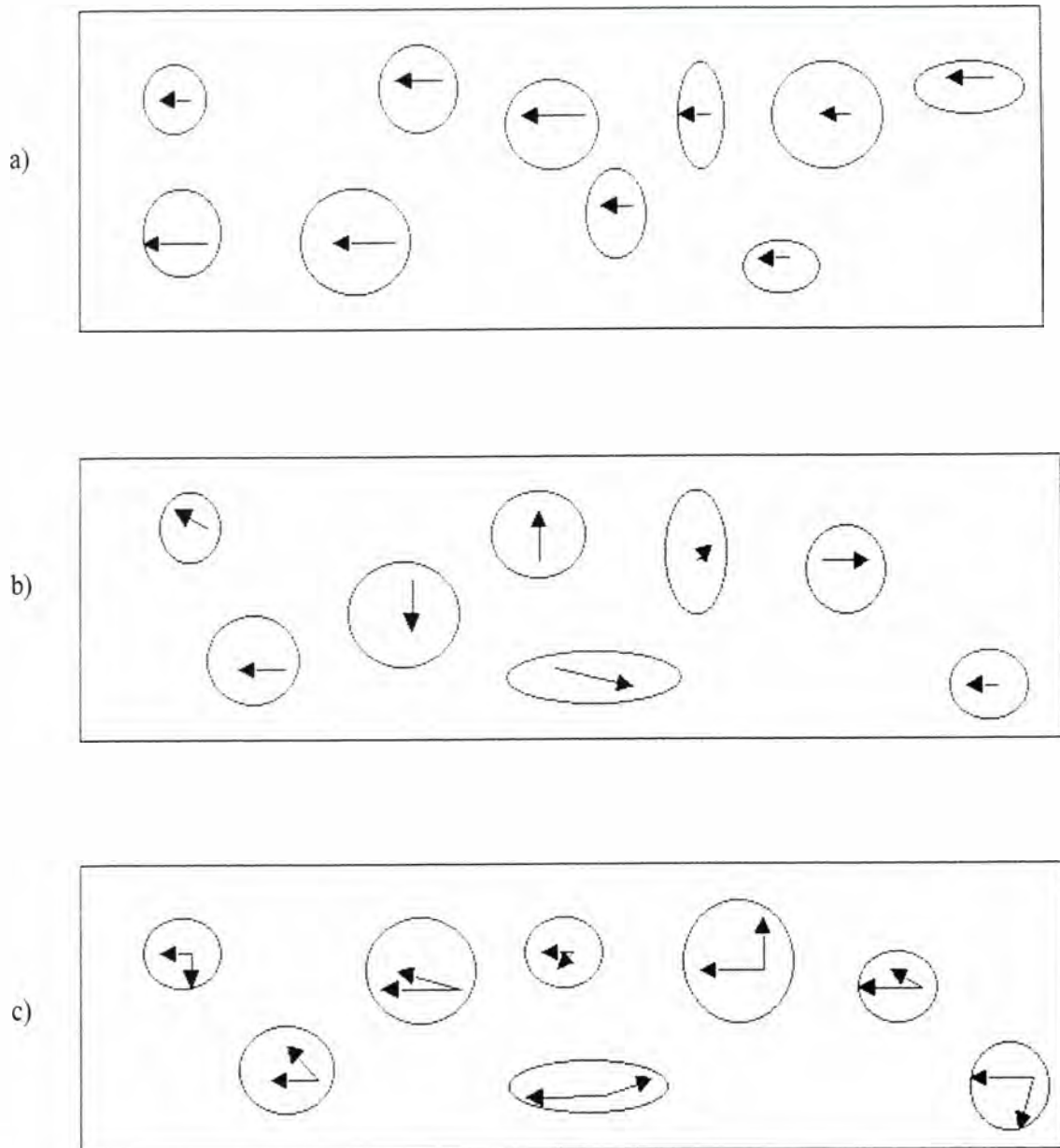
Figure 15: Cartoons of thermal remanent magnetization directions in clasts from volcanic debris flows of different temperatures of deposition. (a) Type I deposit, all clasts emplaced above Curie temperature; (b) Type II deposit, all clasts emplaced below lowest blocking temperature; and (c) Type III deposit, all clasts deposited within their blocking temperature range such that they have a common magnetic component as in a) but also a scattered component as in b).

Anisotropy of Magnetic Susceptibility: Anisotropy of magnetic susceptibility (AMS) techniques were used to determine the preferred orientation of minerals in the rocks. The ellipsoid shape and orientation reflects the overall directional fabric of the sample. The shape ellipsoid with axes K_1, K_2, and K_3 are expressed as the major, intermediate and minor axes respectively. Tuffs commonly have flattening of the AMS ellipsoid parallel to foliation, and the elongation of the ellipsoid is commonly parallel to a fabric lineation (MacDonald and Palmer, 1990). Commonly, K_1 parallels the flow lineations in ignimbrites. K3, the axis of minimum susceptibility, is commonly perpendicular to the plane of flow foliation (Ellwood, 1982).

The KLY-3s Magnetic Susceptibility Bridge was used for measurement. Every specimen collected in the field was measured and the AMS orientations were plotted on equal area diagrams to show the directions of minimum, intermediate, and maximum susceptibility of the sample. Flinn-type plots showing AMS ellipsoid shape were also used to illustrate the shape of AMS ellipsoids.

Rock Composition and Geochemistry

Petrography: Thin sections of the cylindrical cores collected in the field were analyzed for mineral content. Representative samples from the White Chuck Tuff and distal deposits were prepared. Joe Dragovitch of the Washington State Department of Natural Resources also provided thin sections that represented the study sites. Modal analysis was done by counting at least 400 points on each thin section. Ten slides were later stained with sodium cobaltinitrite to evaluate the amount of potassium feldspar present in the samples.

Chemistry: X-ray Fluorescence analysis was done to determine the major and trace element chemistry of thirteen core samples. Each sample was pulverized in a tungsten-carbide ball mill at Western Washington University. Three grams of the powdered samples were combined with 7g of lithium-tetraborate and fused for 10 minutes at 1000° C. Once cooled, the fused glass beads were pulverized and fused again for greater homogeneity. The thirteen samples were sent to Washington State University Geoanalytical lab to be analyzed for major elements and 17 trace elements. Major element and trace element data analysis was done using PetroPlot, a Microsoft Excel based program made available by Yongjun et al (2003).

Results

Paleomagnetism-White Chuck Tuff

Figure 16 represents of the majority of the vector end point diagrams of demagnetized White Chuck Tuff samples taken at sampling locations shown on Figure 14. Nearly all (98%) of the demagnetized tuff samples had similar one-component NRMs. The directions of remanence removed at the higher temperature steps from 400-600° C are well grouped within each site, and between sites. The mean of all White Chuck Tuff site mean directions is declination (dec.) 341.7°, inclination (inc.) 66.5°, $\alpha 95$ 1.7°, and k = 116. Individual White Chuck Tuff site means are listed in Table 1 and shown on equal area plots in Figure 17. Not all 20 samples from each site were used for analysis because statistically the precision of the site mean direction measured with the number of samples used would not increase significantly if all 20 samples were used.

In order to evaluate the magnetic carriers in the samples, three different magnetic mineral measurements were made. Curie temperatures suggest that multiple magnetic minerals are present in the White Chuck Tuff. In Figure 19 three sharp drops are identified along the susceptibility curve at 580°C, 500°C, and 190°C, indicating that the main magnetic carriers are most likely nearly pure magnetite, approximately 20 mol% $TiFe_2O_4$, and approximately 60 mol% $TiFe_2O_4$ (Figure 18) (Dunlop and Ozdemir, 1997). The Lowrie (1990) test of the White Chuck Tuff specimen (Figure 20) presents the range of unblocking temperatures of the low, intermediate, and high field Isothermal Remanent Magnetization (IRM). The magnetization of the IRM components is completely erased

by 500° C. This indicates that high coercivity minerals (>1 T) such as hematite are not present and a small amount of nearly pure magnetite is also present according to the T_c in the White Chuck Tuff.

The White Chuck Tuff contains magnetic minerals that exhibit a wide range of coercivities. The pARM data indicate that the peak in the coercivity spectrum occurs between 2 and 10 mT (Figure 21). This low coercivity range suggests that most magnetite is coarse grained, approximately 5 microns, in the White Chuck Tuff (Jackson, 1988). Opaque minerals observed in thin section have grain sizes ≥ 5 microns (Appendix III). Slightly less remanence is acquired between 10 to 70 mT. This suggests the presence of smaller magnetic grains, which are less abundant in the White Chuck Tuff and have an average grain size of approximately 0.75 microns (Jackson, 1988).

WCT-1-1a

600 C

550 C

500 C

400 C

200 C

NRM

E V
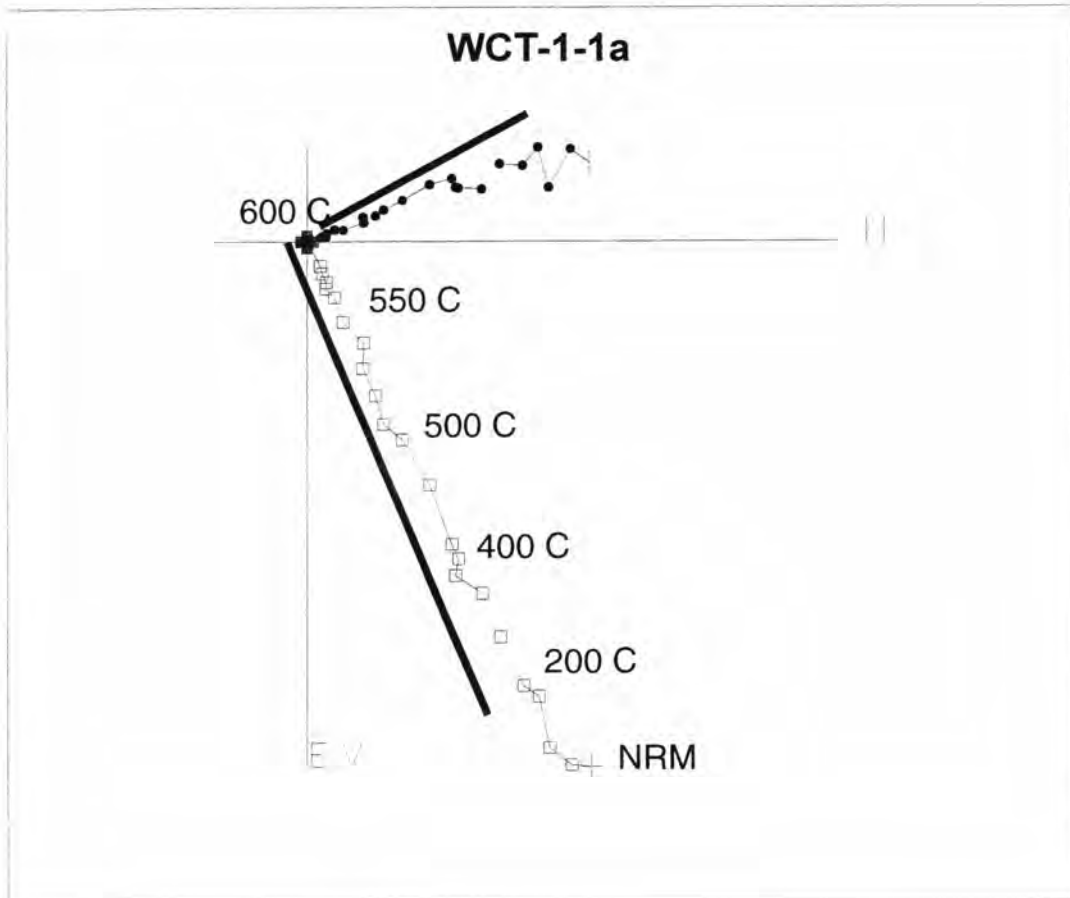
Figure 16. Vector end point diagram of progressive thermal demagnetization typical of the WCT specimens. The filled dircles are projections on the horizontal plane and the open boxes are projections onto the N,E vertical plane. (Tauxe, 1999)

White Chuck Tuff

Site	Declination	Inclination	k	α95	N/N₀	Low unblocking temperature	High unblocking temperature	Latitude / Longitude	VGP Latitude / Longitude	Pole Circle of Confidence
WCT-1	339.3	63.9	602	1.8	12	N/A	400 – 600	48.08N/121.12W	146.6N/75.7E	
WCT-3	347.6	67.2	98	4.4	12	N/A	400 – 600	48.07N/121.12W	166.5N/81.7E	
WCT-4	346.7	67.3	49	6.0	13	N/A	400 – 600	48.08N/121.13W	166.8N/81.7E	
WCT-5	336.6	64.8	292	2.5	12	N/A	400 – 600	48.09N/121.13W	152.7N/74.2E	
WCT-6	339.5	70.1	234	4.0	7	N/A	400 – 600	48.09N/121.14W	181.6N/75.9E	
WCT-7	334.6	66.6	208	3.6	7	N/A	400 – 600	48.10N/121.14W	161.1N/73.3E	
WCT Mean	340.6	66.7	720	2.5	6	N/A	N/A		77.2N/161.4E	D_p – 3.4 D_m – 4.1

Distal Deposits

Site	Declination	Inclination	k	α95	N	Low unblocking temperature	High unblocking temperature	Latitude / Longitude	VGP Latitude / Longitude	Pole Circle of Confidence
WC-1 Low	341.4	78.2	24	8.4	14	150 – 375	375 – 570	48.10N/121.27W	219.1N/68.6E	D_p – 14.9 D_m – 15.8
SR-1 Low	157.2	36.2	3	34.3	12	150 – 325	325 – 500	48.14N/121.35W		
SR-2 Low	150.6	-4.3	3	70.1	4	150 – 300	325 – 500	48.17N/121.34W		
SR-3 Low	301.0	51.6	4	28.8	9	150 – 250	250 – 550	48.16N/121.36W		
ST-1 Low	244.5	88.7	1.7	77.5	6	150 – 250	250 – 500	48.16N/121.40W		

Table 1. Magnetic site mean directions, statistics, number of samples, and unblocking temperatures used for the White Chuck Tuff and distal deposit paleomagnetic study. WC-1 was the only distal site with well-defined magnetic pole directions.

WCT-1 WCT-3 WCT-4

WCT-5 WCT-6 WCT-7
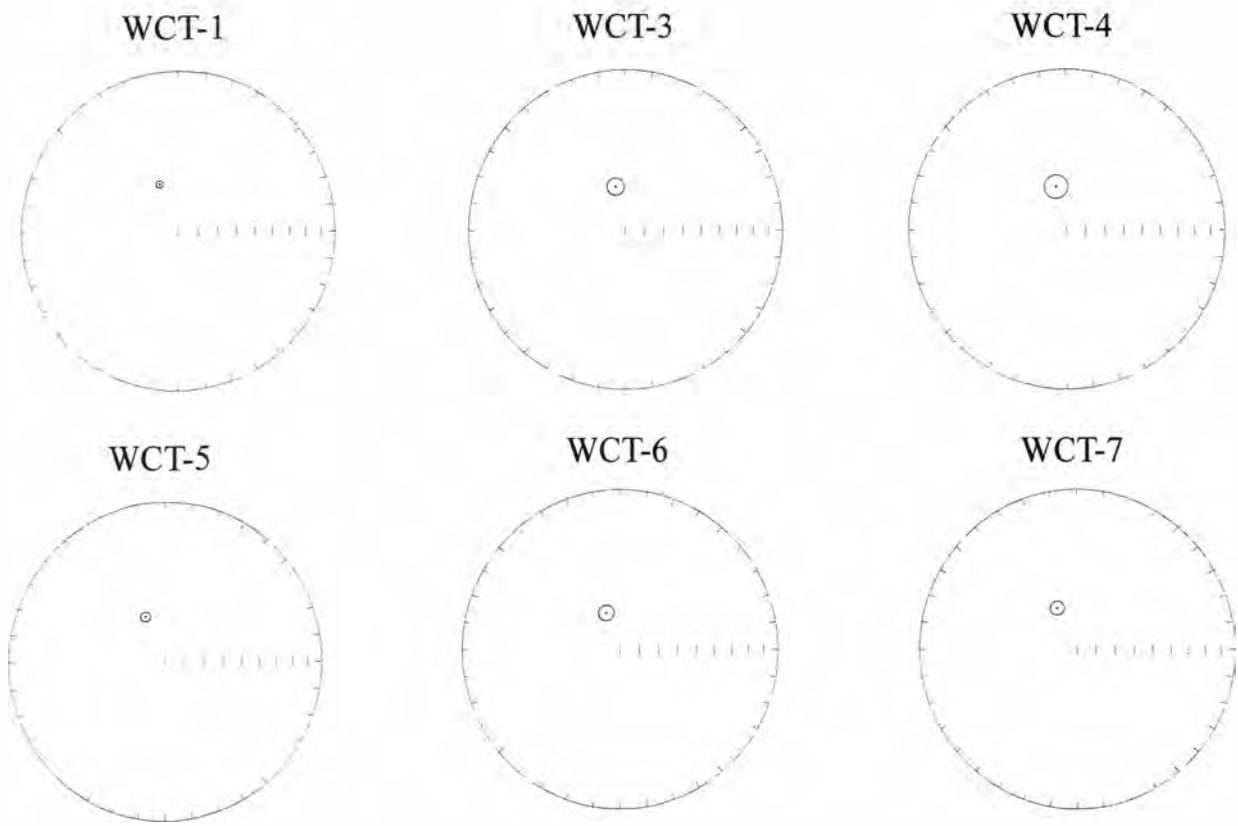
Figure 17. Equal area diagrams of site mean directions from the six White Chuck Tuff sites of Table 2. (Tauxe, 1999)
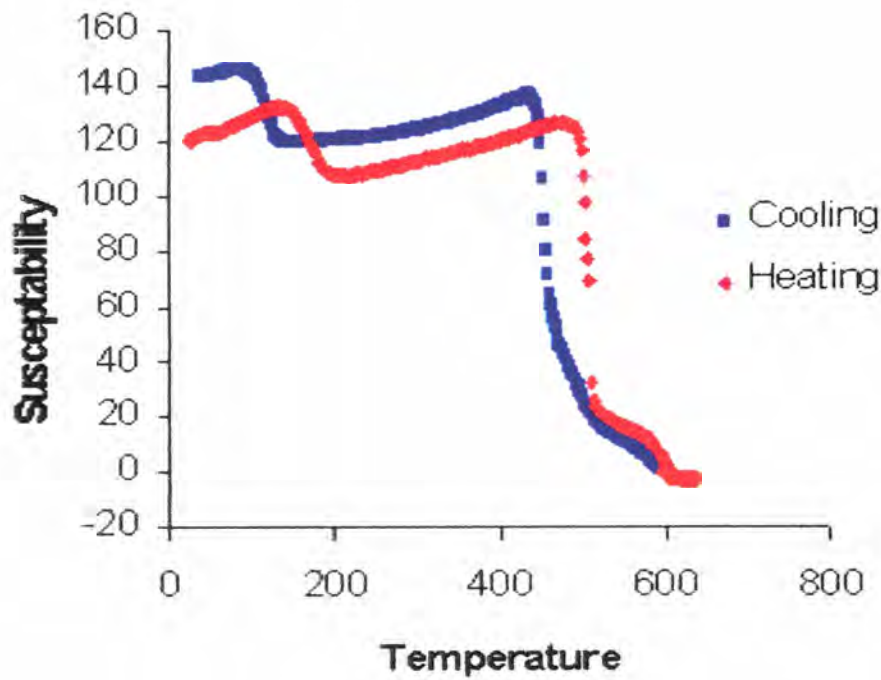
Figure 18. Plot of Susceptibility versus Temperature for a typical White Chuck Tuff specimen. The "intersecting tangents" method was used to determine the magnetic mineral associated with the approximate unblocking temperature found which is approximately 190, 500, and 590 degrees C.
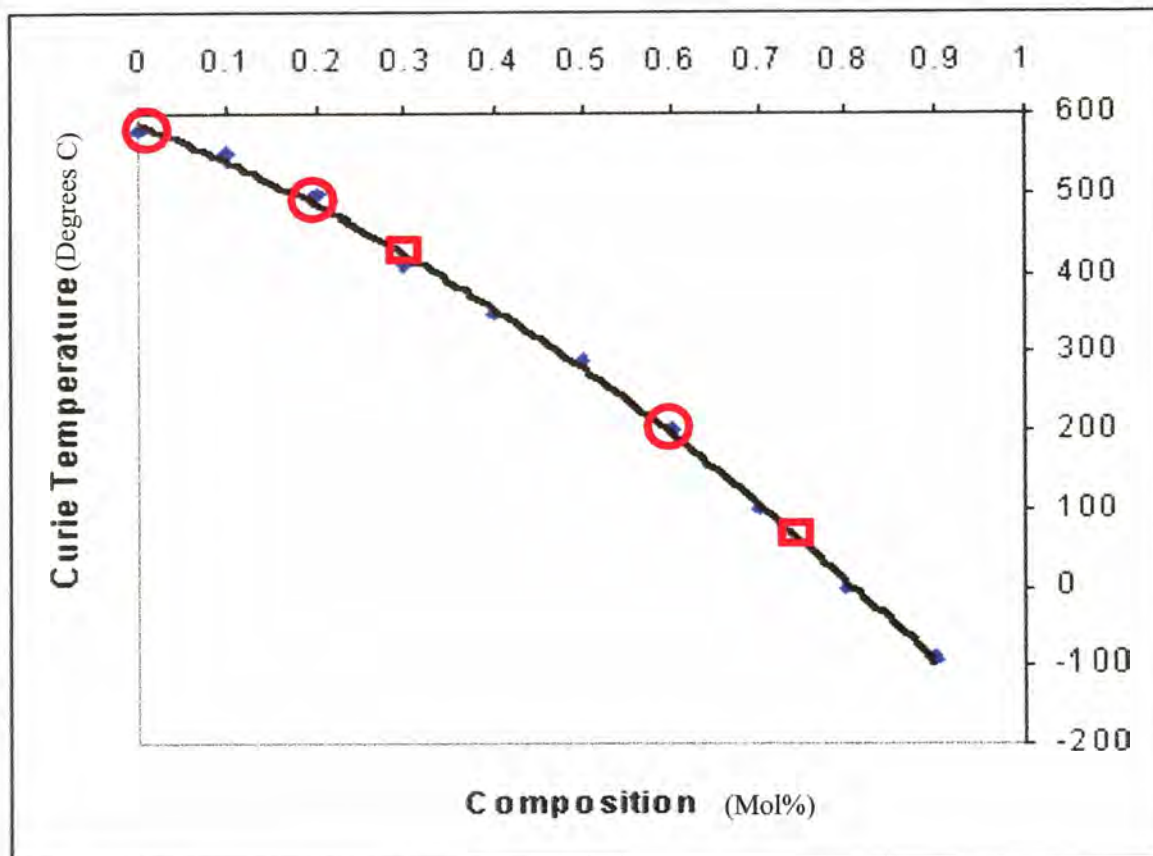
Figure 19. Curie Temperature versus mole percent of the ulvospinel-magnetite solid solution series. The trendline is taken from Dunlop and Ozdemir, 1997, and the open circles are the compositions of the titanomagnetite and magnetite in the White Chuck Tuff, and the open squares are the compositions of the titanomagnetites in the distal deposit dacite clasts. The temperature data are taken from Curie Temperature curves of a White Chuck Tuff sample and a distal deposit vesicular sample. The White Chuck Tuff Curie Temperature curve had three changes in susceptibility at the temperatures indicated above and the distal deposit Curie Temperature curve had two changes in susceptibility at the temperatures indicated above.

WCT 4-1
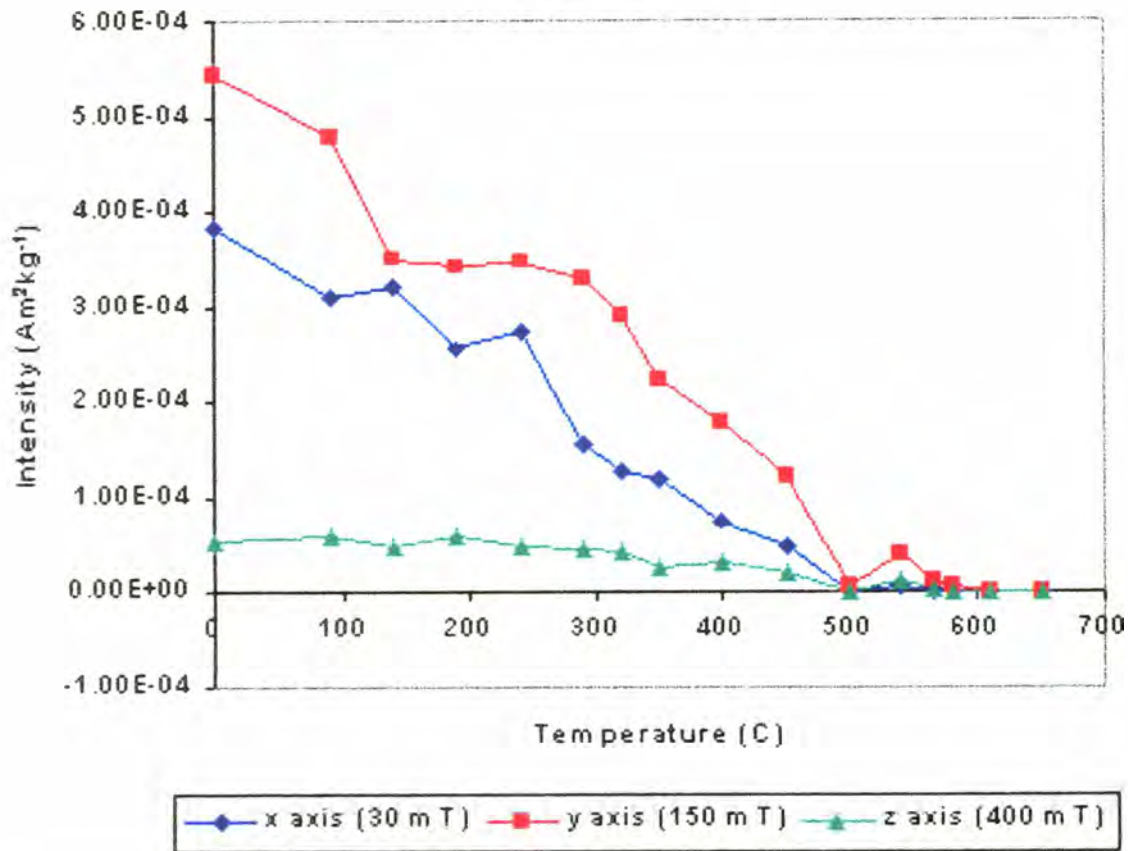
Figure 20. White Chuck Tuff specimen demagnetized using the Lowrie method. This graph indicates that all of the magnetization is lost before 500 degrees C. The bulk of the remanence is in magnetic grains with coercivities between 30 and 150 mT, and very little remanence is acquired in the high coercivity grains.
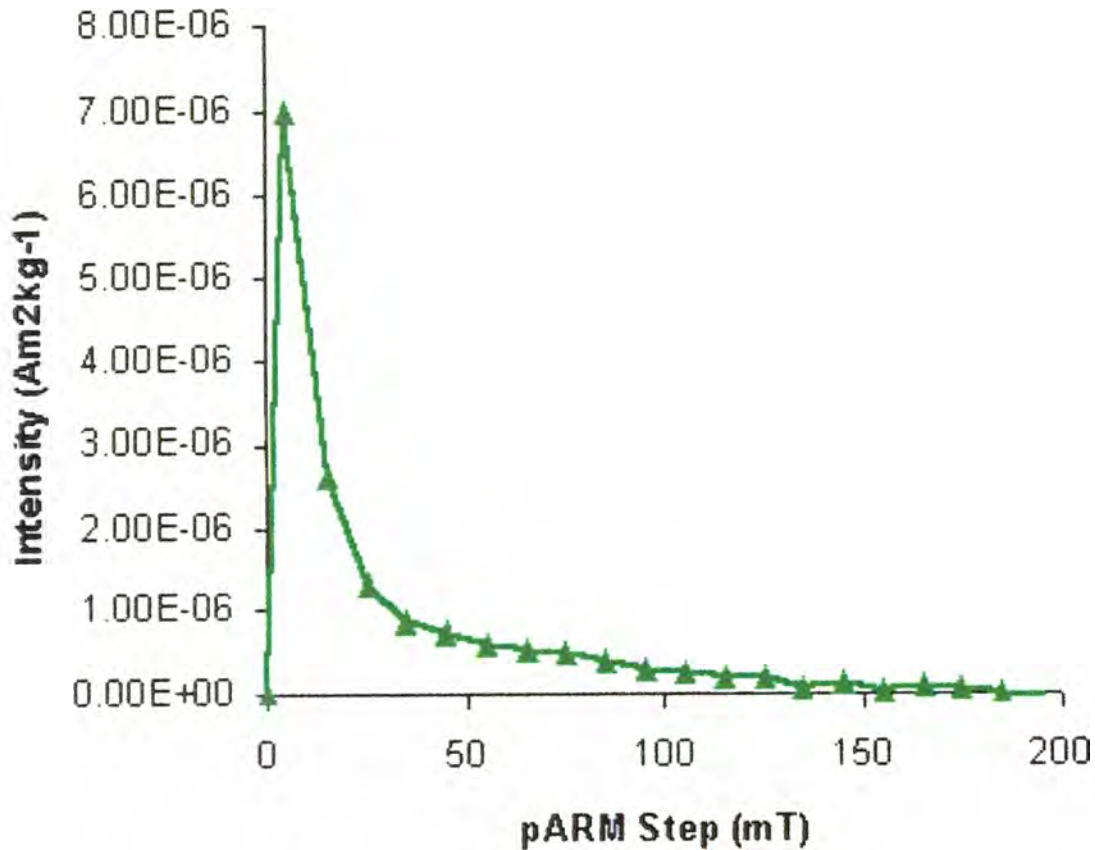
Figure 21. pARM plot of a White Chuck Tuff sample showing the high coercivity measurements in the 1-25 mT range. This indicates that the prominant carrier of the magnetic remenance are grain sizes of 5-0.75 microns in the White Chuck Tuff. These larger grain sizes most likely indicate magnetic carriers of multi-domain and pseudo single domain magnetite and/or titanomagnetite (Jackson, 1988).

Paleomagnetism-Distal Deposits

Clasts found in the distal deposits have two distinct lithologies: vesicular and non-vesicular dacite. Not only are the clasts distinct lithologically but paleomagnetically. All specimens of the distal deposits have at least two components of magnetization, a low unblocking temperature component and a high unblocking temperature component (Figure 22).

The low unblocking temperature NRM component was better defined (MAD<15) than the high unblocking temperature component (MAD < 30) for most specimens. The distal deposit low temperature component site means are shown in (Table 1 and Figure 23). Methods of Fisher (1953) were used to obtain the site mean directions and $\alpha 95s$ for the distal deposits, WC-1, SR-1, SR-2, SR-3, and ST-1. The site means of three of the five sites have site means in the NW quadrant. Sites SR-2 and SR-3 do not plot near the other four distal sites. Figure 24 compares the directions of the low and high unblocking temperature components of the distal deposits. This difference between components is an indication that there are significant differences in magnetization between low unblocking temperature and high unblocking temperature components. All the distal deposits display this characteristic.

The temperature at which the low unblocking temperature component was unblocked varies from site to site. Sites SR-1, SR-2, SR-3, and ST-1 have unblocking temperatures between 200°C and 300°C. These temperatures are lower then the Curie temperature of the majority of magnetic minerals that make up the clasts. These distal deposits show Type II deposit characteristics. Site WC-1 is the most proximal of the

41

distal sites and the low unblocking temperature is unblocked at approximately 375° C. The warmer unblocking temperature of WC-1 suggests that this is a Type III deposit.

The magnetic mineralogy identified by 580° and 460° C Curie temperatures of distal deposit samples are magnetite and titano-magnetites (Figure 25 and Figure 18) (Dunlop and Ozdemir, 1997). The Lowrie (1990) test (Figure 26) measurements show that the minerals have unblocking temperatures at approximately the same temperatures as the Curie temperature, 440° and 580°C. The Lowrie test also points out the difference in non-vesicular and vesicular dacite specimens. The remanence acquired by minerals with coercivities in the two lower ranges is similar for vesicular specimens. A relatively higher proportion of grains have intermediate coercivities, from 30 to 150 mT, in the non-vesicular specimen.

Figure 27 displays the range of coercivties of magnetic minerals present in the two lithologies of distal deposits' vesicular and nonvesicular specimens. The pARM data for the vesicular specimen, from ST-1, show that the low coercivity grains mostly dominate the magnetization. A relatively larger amount of high coercivity grains appear to contribute to the magnetization in the nonvesicular specimens, SR-3.
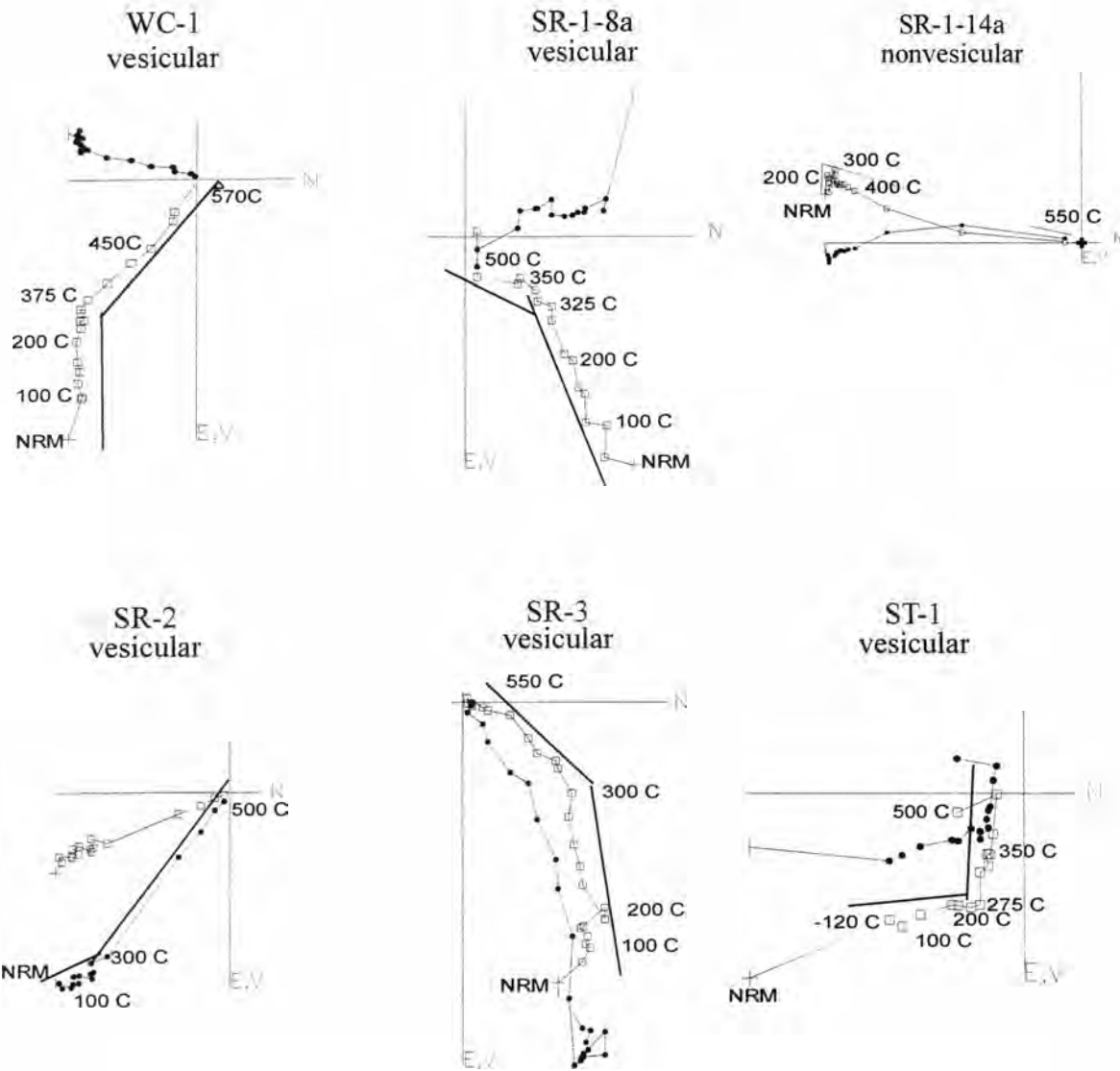
Figure 22. Vector end point diagrams for progressive thermal demagnetization of vesicular and nonvesicular specimens from the distal deposits. In these examples the inflection points are between 250 and 350 degrees C much lower then the White Chuck Tuff specimens. The nonvesicular clast of SR-1-14a clast show upward directions, which is the case in most of the distal site nonvesicular clasts. WC-1 was the only site to have a well grouped site mean. (Tauxe, 1999)

Low Unblocking Temperature
Component

High Unblocking Temperature
Component

WC-1

SR-1

SR-2

SR-3

ST-1
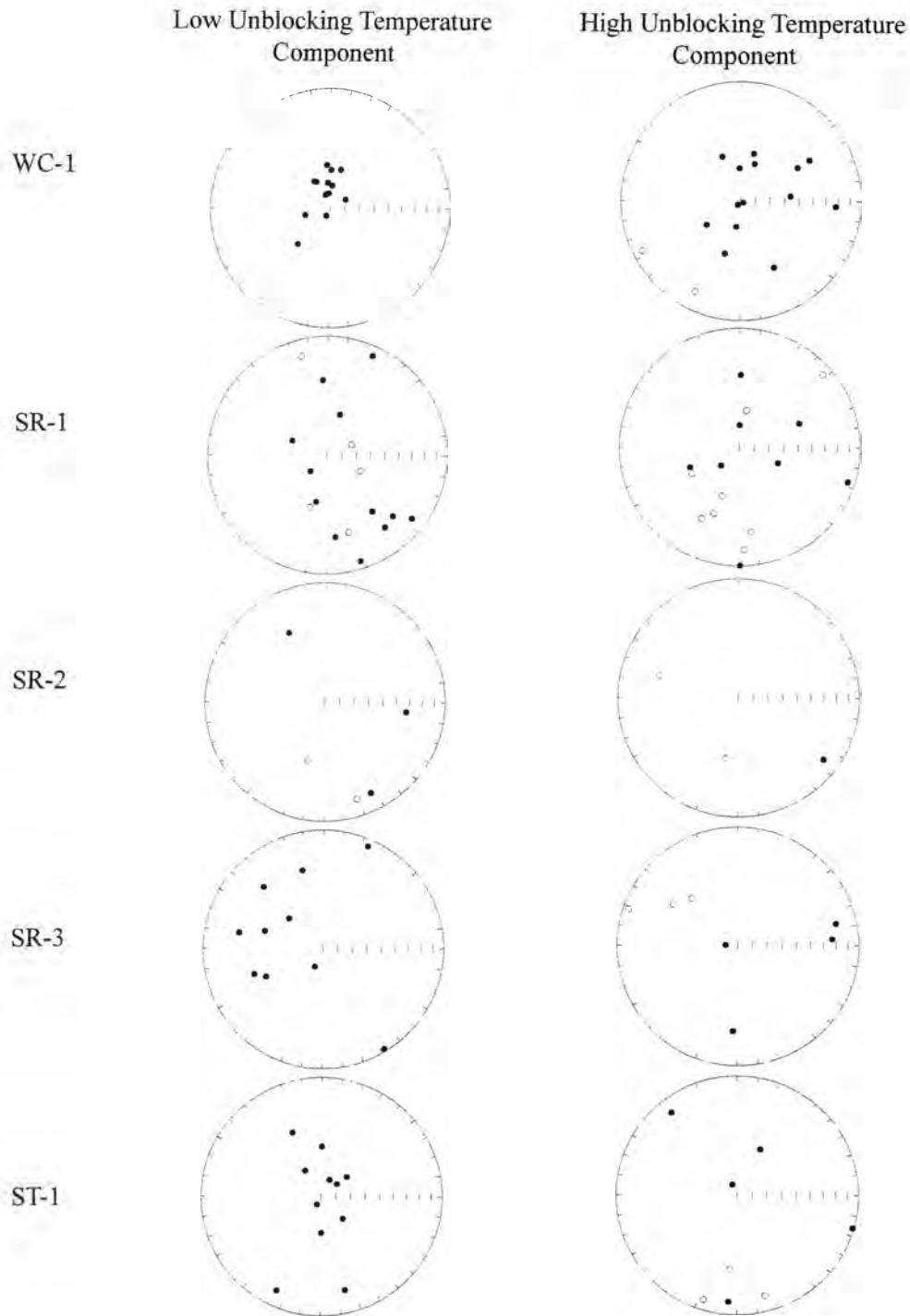
Figure 23. Equal area projections of the low and high temperature removed components
of the distal deposits. The directions of the components in the low temperature
range appear to be clustered, whereas the directions of the components in
the high temperature range appear to be dispersed compared to the low
temperature components. (Tauxe, 1999)

44

WC-1

SR-1

SR-2

SR-3

ST-1
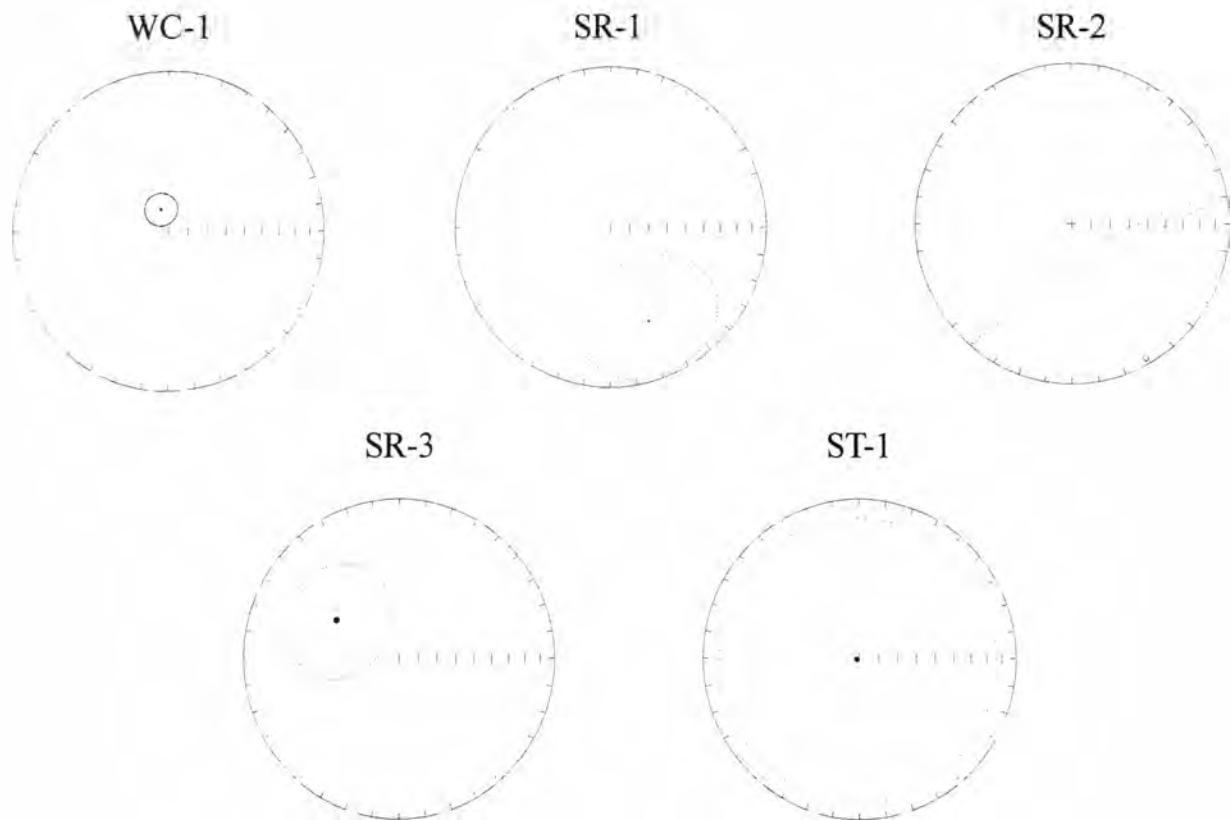
Figure 24. Equal area diagrams of site mean directions from the five distal deposit
sites of Table 1. (Tauxe, 1999)
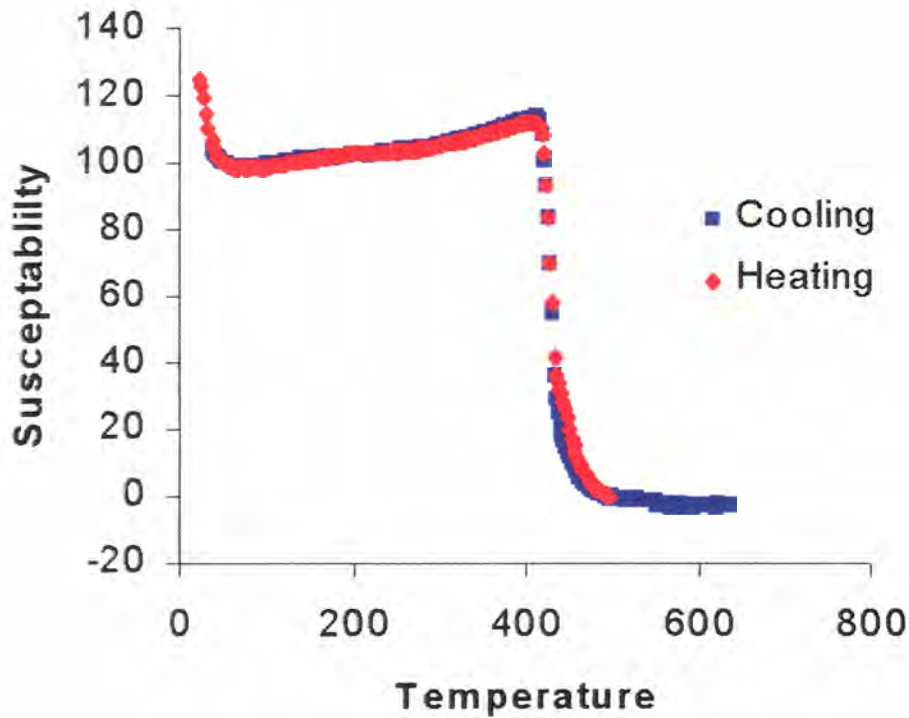
Figure 25. Susceptibility versus Temperature diagram of a specimen from site ST-1. The "intersecting tangents" method was used to determine the Curie Temperature which is approximately 70 and 440 degrees C. This suggests that the magnetic mineral is a titanomagnetite with about 80% and 30% TiO2 respectively. The heating and cooling curves are very similar, which indicates that a minor amount of alteration occurred during the measurement process.
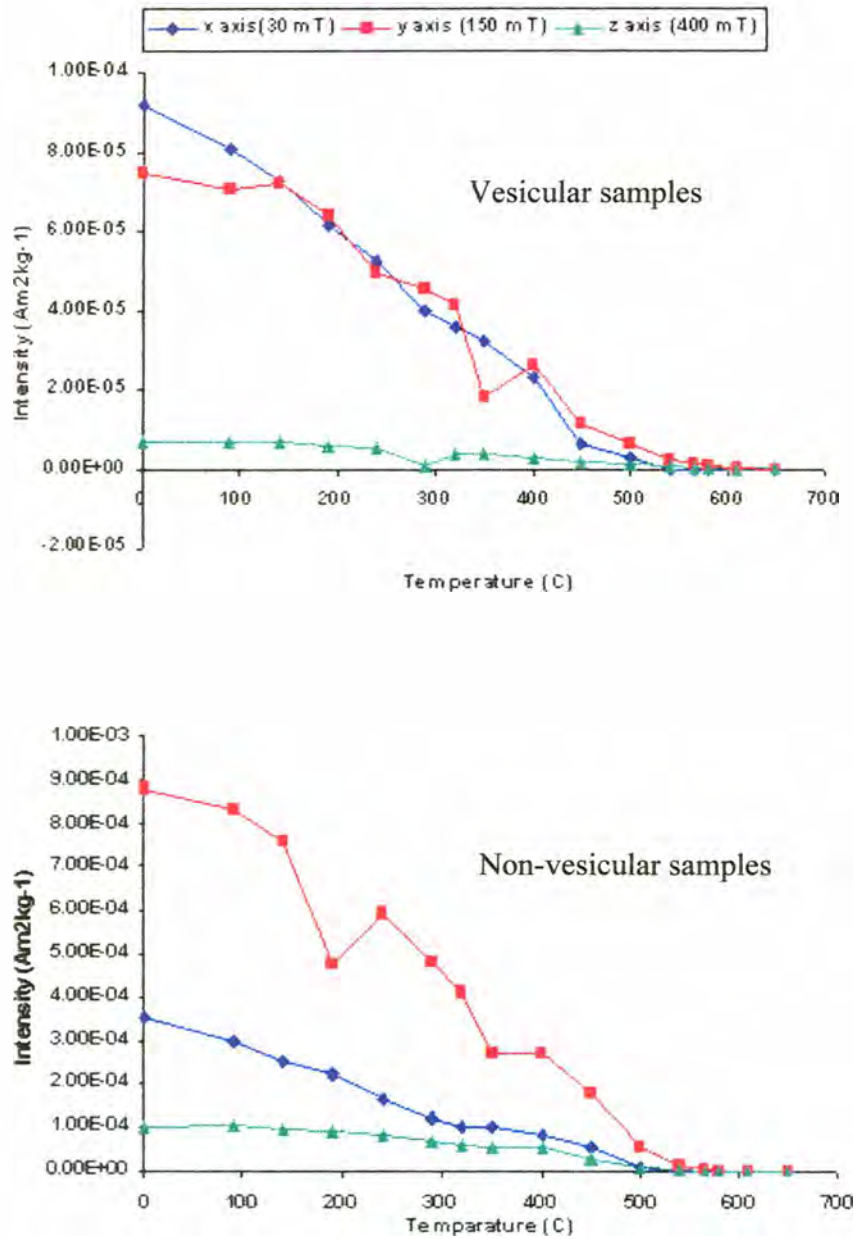
Figure 26. Two examples of distal deposit samples subjected to demagnatization using the Lowrie test. The top graph is of a vesicular sample and the bottom graph is of a non-vesicular sample. The diagrams show distributed unblocking temperatures of magnetization from 0 to 30 mT, from 30 to 150 mT, and from 150 to 400 mT. The the total magnetization has been effectively unblocked between 550 and 600 degrees C. This is consistant with the lack of hematite in the samples and a low contribution of the highest IRM. The difference between the samples is that there is a higher contribution of intermediate IRM influence in the non-vesicular sample than in the vesicular sample.

47

ST-1   SR-3

Vesicular   Non-vesicular
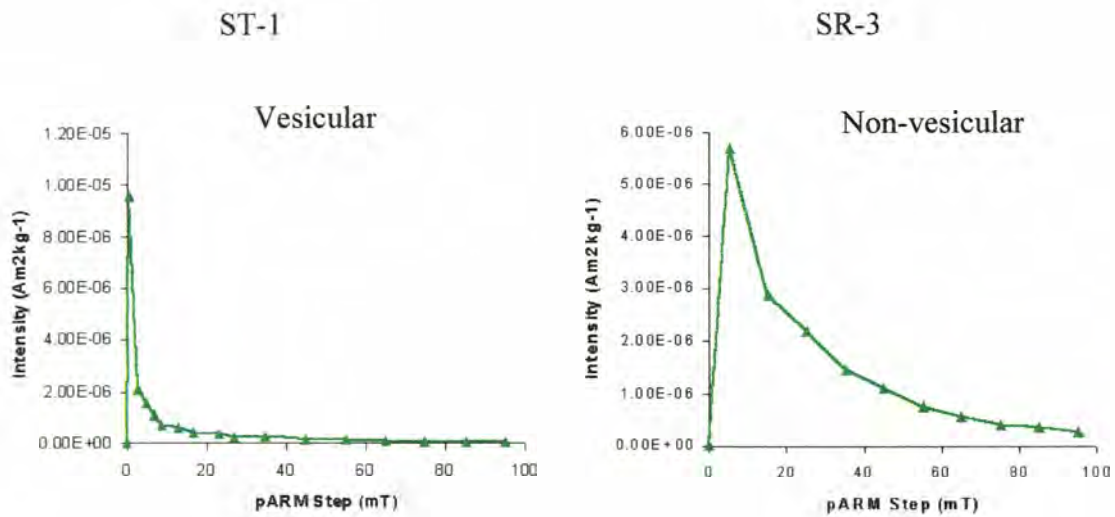
Figure 27. pARM plots of a vesicular dacite sample from ST-1 (left) and a non-vesicular
dacite sample from SR-3 (right). The diagrams show that the low coercivity
grains mostly dominate the magnetization in the samples but in the non-vesicular
sample there is a relatively larger amount of high coercivity grains contributing to
the magnetization.

48

Anisotropy of Magnetic Susceptibility

Flinn type plots show ellipsoid shape (Flinn, 1962) for all samples collected from the White Chuck Tuff and distal deposits (Figure 28). The Flinn plots of the White Chuck Tuff, sites WCT-1 through WCT-7, show that the ellipsoids are dominantly oblate with low anisotropy, $P \approx 1.02$. The tuff from site SR-1 has oblate AMS ellipsoids and is similar to the White Chuck Tuff sites. Visually the distal deposit specimens have different ellipsoid shapes than the White Chuck Tuff. The pumiceous samples from site WC-1 have mostly prolate AMS ellipsoids. The pumiceous samples from sites SR-1 and ST-1 have AMS ellipsoids that have both prolate and oblate shape. The non-vesicular samples are mostly oblate.

The AMS ellipsoids for the White Chuck Tuff have tightly clustered minimum axes and less-well clustered (but significant) intermediate and maximum susceptibility axes (Figure 29). This is consistent with the dominant oblate fabric pattern in the Flinn diagrams. The confidence ellipsoids about the site mean minimum axes do not include the vertical direction, which is consistent with imbrication of the oblate fabric.

Equal area plots of the AMS data in the distal deposits show the scattered distribution of magnetic fabrics. In the distal deposit sites the K3 directions are all scattered (Figure 30). The separation of the anisotropy data by clast types has similar scattered results. The important distinction between the White Chuck Tuff and the distal deposits is that the distributions of K_3 pole directions, in the distal deposits, do not cluster in any significant way.

49
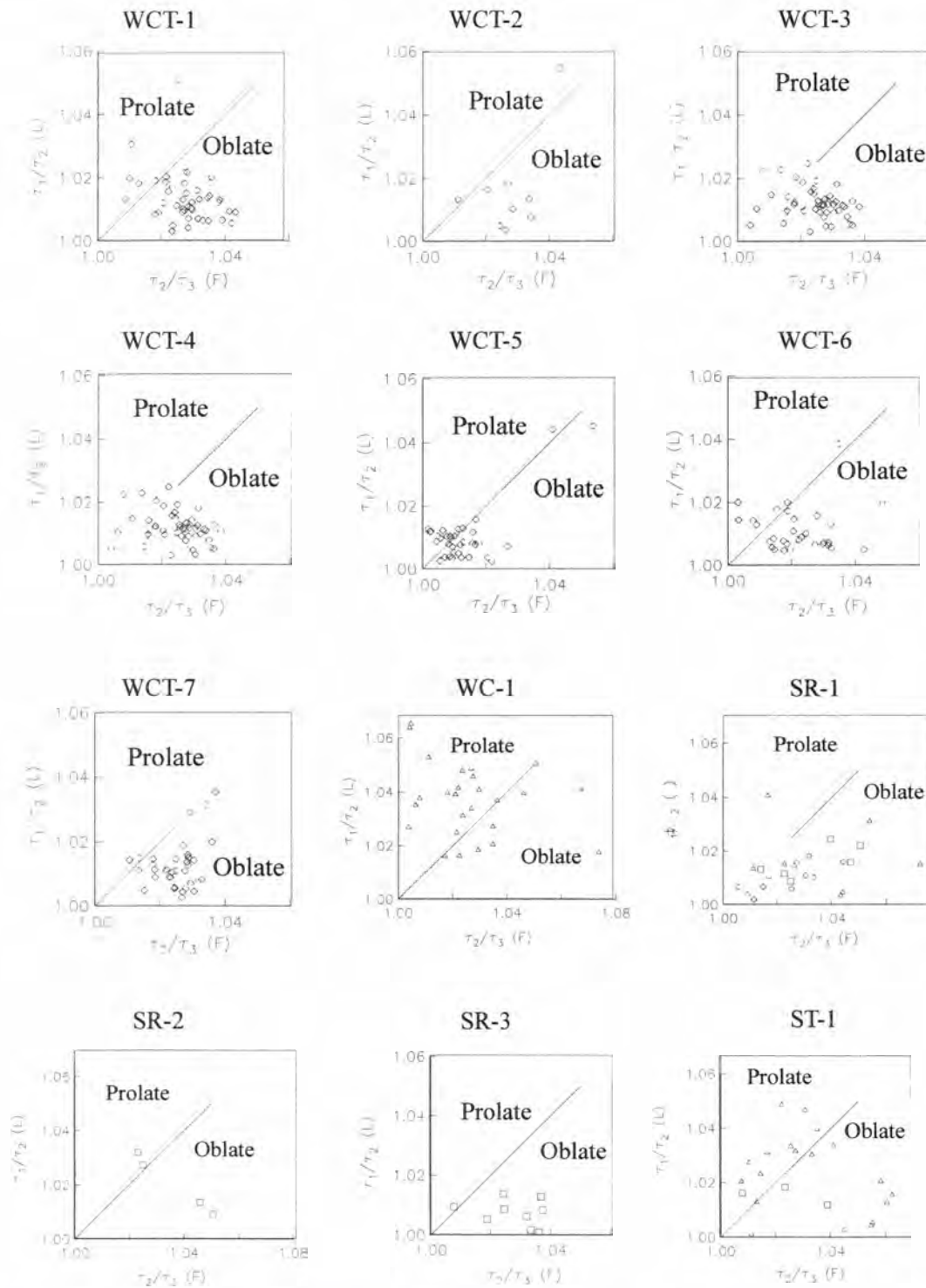
Figure 28. Lineation versus Foliation Anisotropy of Magnetic Susceptibility (AMS) diagrams of this study with the corresponding site number indicated.(Tauxe, 1999)

(White Chuck Tuff = diamonds, Vesicular clasts = triangles; Non-Vesicular clasts = squares)

50

Figure 29. Representative Anisotropy of Magnetic Susceptibility (AMS) equal area plots of this study with the site number indicated (K1 (square), K2 (triangle), K3 (circle)). WCT-1, WCT-2, WCT-4, WCT-6 and WCT-7 show down valley flow directions based on the Southeast dipping imbrication (Figure 12). WCT-5 shows no significant dip. WCT-3 shows a minor SW dipping imbrication. A "p" was used for the calculation of confidence elipsoids. (Tauxe, 1999)

51
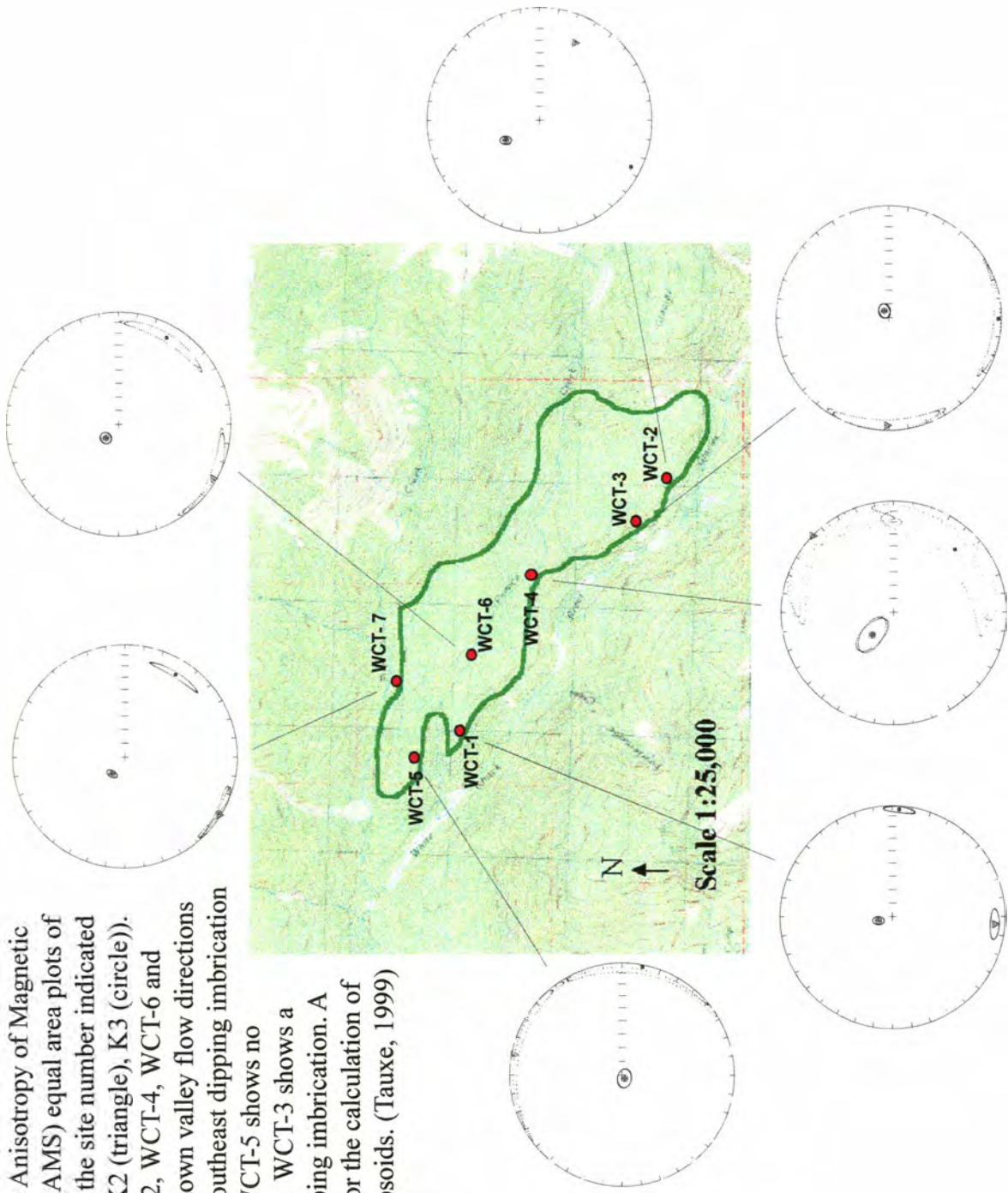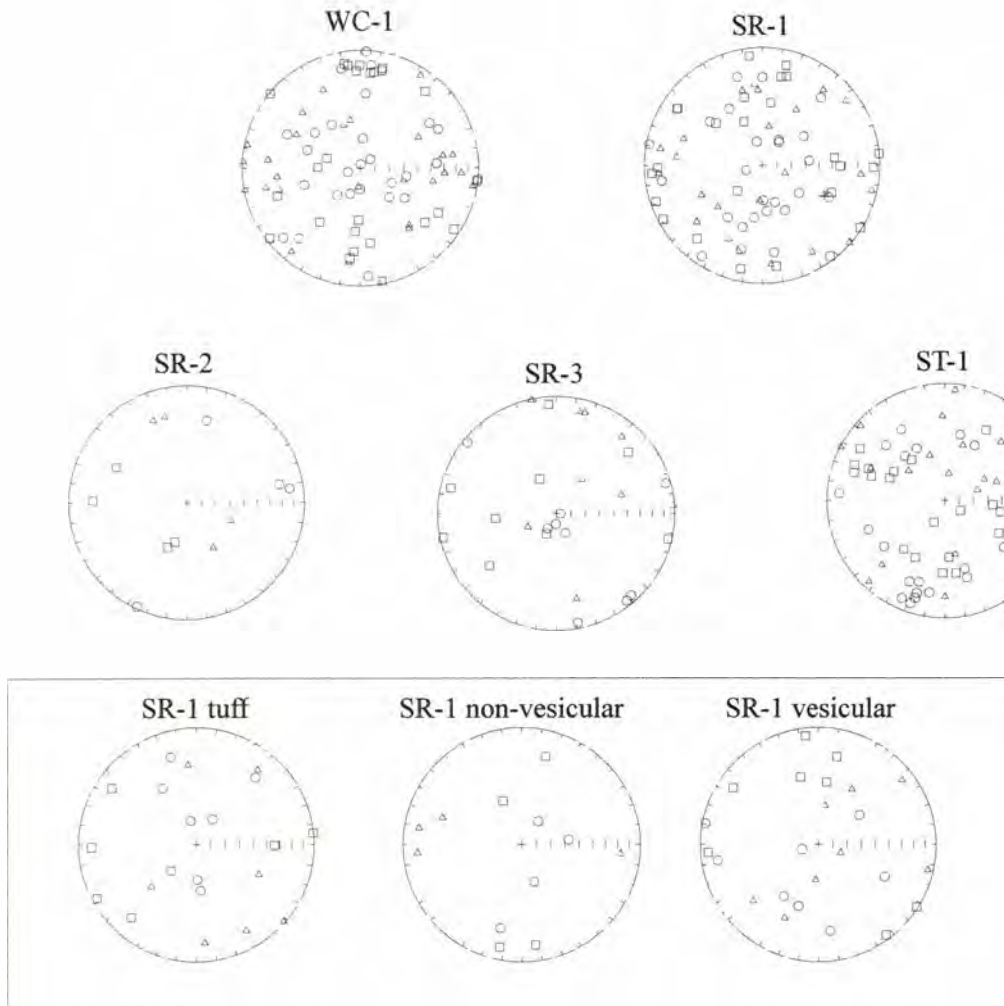
Figure 30. Representative Anisotropy of Magnetic Susceptibility (AMS) equal area plots of this study with the site number indicated (K1 (square), K2 (triangle), K3 (circle)). AMS plots of the distal deposits do not have defined magnetic fabrics. Deposit SR-1 has been subdivided into clast lithology for comparison. Notice the tuff samples do not share the same fabric orientation as the WCT sites. The non-vesicular and vesicular clast samples also show independent orientation amongst each individualsample. (Tauxe, 1999)

Petrography

Thirteen thin sections were used to identify the mineralogy of the clasts and distinguish differences between collection sites and non-vesicular/vesicular clasts (Appendix III). All thin sections had at least 400 points counted including matrix, voids, and phenocrysts. The phenocrysts observed in the samples were plagioclase feldspar, hornblende, orthopyroxene, clinopyroxene, oxyhornblende, and opaque minerals. In Figure 31 point count data are depicted in radial charts to display differences and similarities of the six Glacier Peak deposits studied. Identifying the mineralogy of the White Chuck Tuff and the distal deposits should show similar composition if from a similar magma system. The phenocrysts used for these charts are hornblende (Figure 32), oxyhornblende (Figure 33), hypersthene (orthopyroxene) (Figure 34), clinopyroxene (Figure 35), and opaque minerals. The matrix, voids, and feldspar point counts were similarly abundant in all samples and would not show the minute differences of Fe-Mg minerals (Appendix III). The filled area, in Figure 31, of the five deposits, WCT-3, WC-1, SR-1, SR-3, and ST-1 have similar distribution patterns even though the number of phenocrysts counted in a particular sample differ between sites. The White Chuck Tuff deposit is represented by WCT-3 because all of the WCT samples are similar and would produce the same chart shape. All deposits except for SR-2 have a significantly greater amount of hornblende than the other minerals, whereas SR-2 is noticeably different in shape, due to the occurrence of oxyhornblende and a high abundance of opaque minerals. Clinoproxene was observed in similar proportions at each deposit. The matrix of most specimens has been altered to potassium rich clay due to devitrification of the glass.
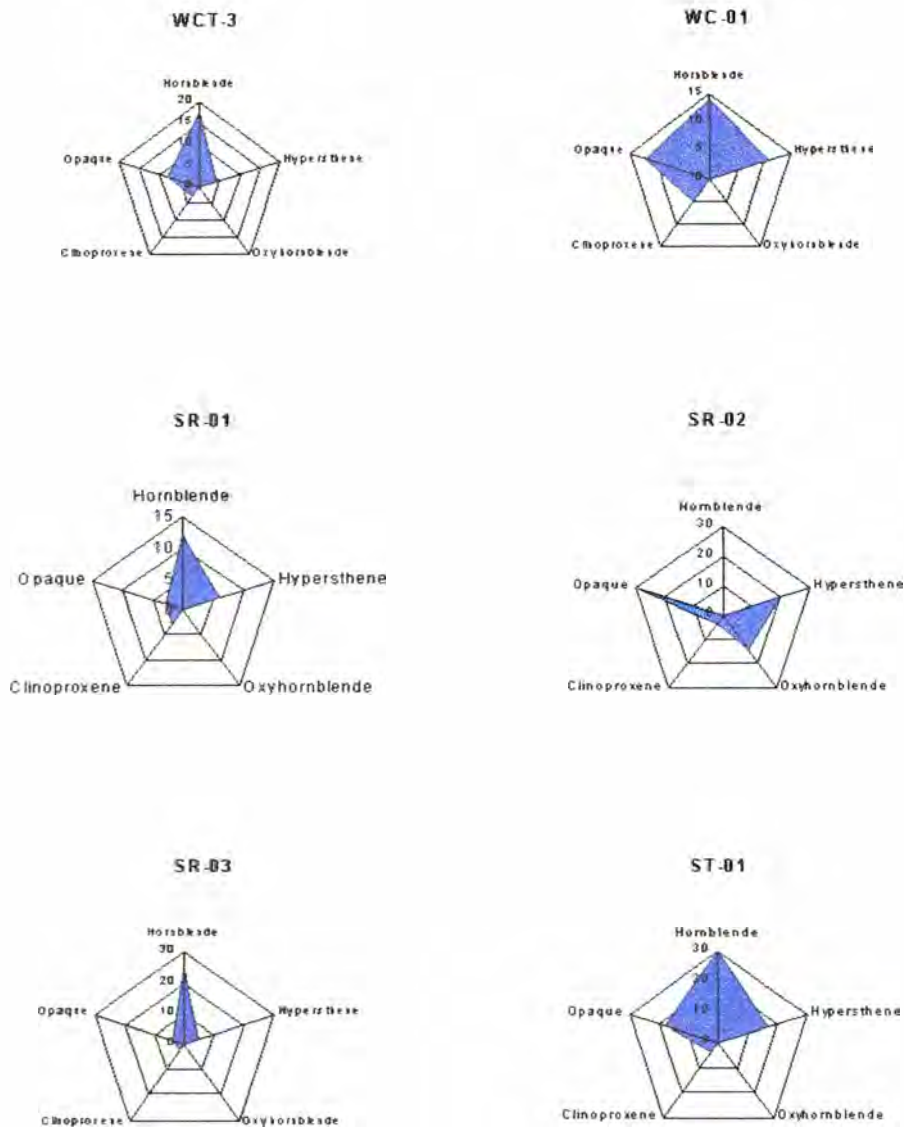
Figure 31. Shown above are radial charts depicting the number of points counted in thin sections of Fe-Mg minerals collected from the six Glacier Peak deposits in this study. The radii of the chart represent the minerals present and the filled areas are the number of points counted.

Figure 32. In center of view is a hornblende (Hb) crystal in crossed polarized light (XPL) surrounded by twinned feldspar. The pseudohexagonal cross section of the hornblende displays its characteristic cleavage angles.
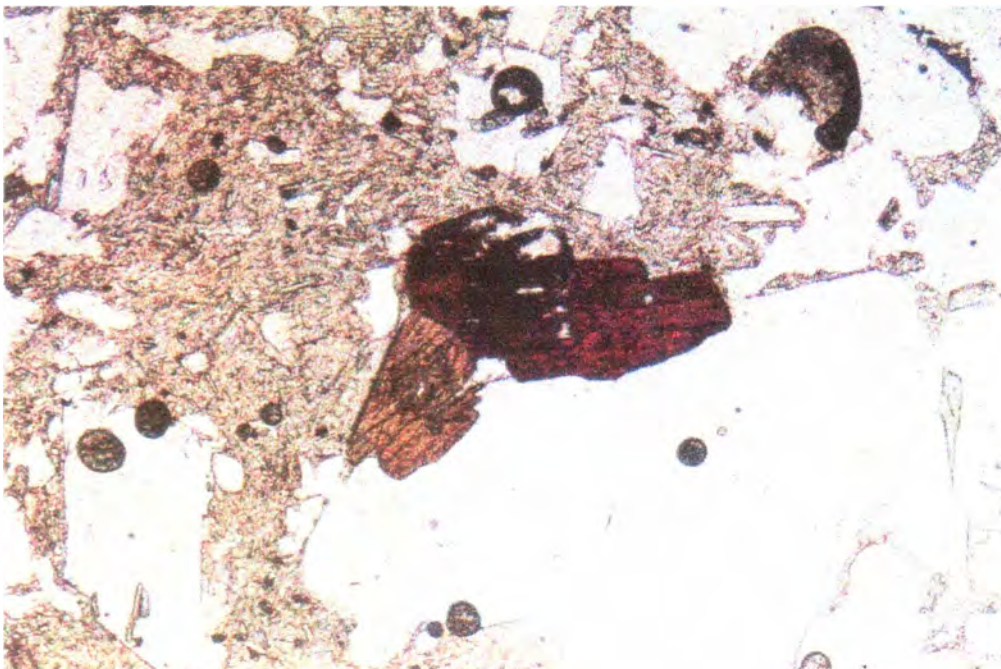
Figure 33. In center view is an example of an oxyhornblende in plain polarized light (PPL) (site SR-2). The oxyhornblende has a distinct red pleochroism and parallel extinction.

55
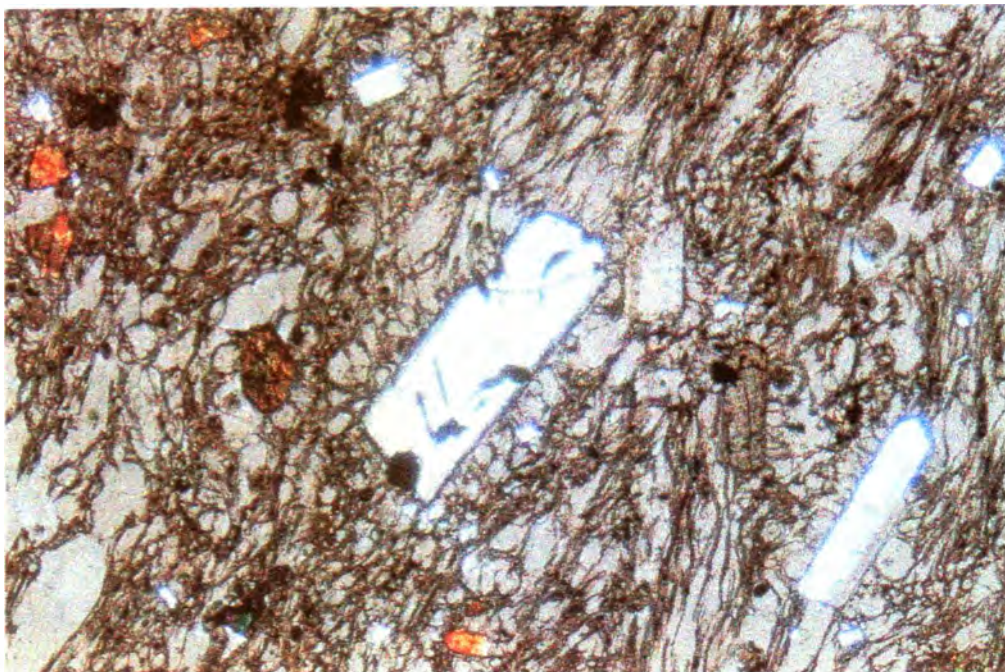
Figure 34. A hypersthene phenocryst (center) in plane light at approximately a 45 degree angle from vertical where it is not extinct. The phenocryst is in a vesicular sample. Minor alteration of the glassy texture was observed. Note: Hypersthene is present all six deposits.

Figure 35. A clinopyroxene phenocryst (augite) in a vesicular sample in XPL. The phenocryst (center) has inclined extinction and similar examples of clinopyroxene can be found in the other five deposits.

Chemistry

The chemical data displayed in Table 2 are representative of the six deposits. The data were used for comparison of the White Chuck Tuff and distal deposits. Pumice clasts were used for chemical analysis in this study.

The total alkali vs. silica diagram (TAS diagram) (Figure 36) shows the whole rock composition of the 10 samples analyzed. The chart shows that the samples are subalkaline, of dacite composition. The samples grade from the least felsic samples, WCT-4, 6, and 7, to the most felsic samples, ST-1 and one sample of SR-1.

Figure 37 is major element versus silica diagrams. The diagrams display variations with increasing silica typical of calc-alkaline magma suites. The plots show that Al_2O_3 and Na_2O increase as silica increases and TiO_2, FeO_3, CaO, and MgO decrease as silica increases. Figure 38 shows trace element versus silica diagrams that display no distinct difference among the samples analyzed, but some clustering of individual deposits. Figure 39 is a variation diagram of the ratios, Zr/Ti versus Sc/V. The White Chuck Tuff samples plot close together whereas the distal deposits are scattered over the Sc/V ratio and have similar Zr/Ti ratios. Dense clustering of deposits does not occur nor do any distal deposit samples cluster around the White Chuck Tuff.

	WCT-4 15b	WCT-6 12b	WCT-7 16b	WC-1 5B	WC-1 15B	SR-1 6B	SR-1 8B	SR-1 15B	SR-2 2T	SR-3 38B	ST-1 12b	ST-1 4a	ST-1 13B
Normalized Major Elements (Weight %):													
SiO2	64.58	64.22	64.23	66.14	66.38	64.98	67.67	65.13	64.27	64.94	66.45	66.90	67.12
Al2O3	17.48	17.95	17.64	17.84	17.33	17.56	16.65	16.84	17.12	17.36	17.29	16.54	16.62
TiO2	0.572	0.583	0.583	0.546	0.576	0.565	0.486	0.615	0.581	0.608	0.517	0.531	0.502
FeO*	3.86	3.88	3.93	3.19	3.62	3.71	2.99	3.88	4.03	3.98	3.35	3.26	3.41
MnO	0.080	0.080	0.081	0.067	0.073	0.077	0.065	0.082	0.082	0.079	0.072	0.072	0.078
CaO	4.97	4.91	5.09	4.22	4.03	4.79	3.90	4.73	5.07	4.54	4.04	4.12	3.84
MgO	2.48	2.44	2.48	1.99	2.07	2.41	1.79	2.62	2.71	2.52	1.99	1.97	2.08
K2O	1.61	1.61	1.58	1.81	1.87	1.64	2.17	1.92	1.85	1.91	2.02	2.23	2.10
Na2O	4.21	4.16	4.24	4.05	3.89	4.11	4.14	4.02	4.15	3.90	4.14	4.23	4.11
P2O5	0.151	0.152	0.152	0.153	0.160	0.157	0.132	0.152	0.144	0.165	0.135	0.138	0.133
Unnormalized Trace Elements (ppm):													
Ni	18	21	18	16	13	18	12	20	27	19	16	16	15
Cr	21	23	22	17	17	22	14	27	23	27	18	16	28
Sc	9	8	7	4	7	8	5	2	12	10	8	3	5
V	91	97	78	79	84	83	69	93	90	93	69	70	75
Ba	440	451	436	521	508	463	548	495	458	489	520	561	527
Rb	31	30	33	35	35	30	44	37	33	38	39	45	42
Sr	606	598	614	596	544	592	413	429	470	468	434	416	408
Zr	128	128	134	145	152	130	133	133	125	143	134	137	121
Y	14	13	13	12	14	14	14	16	14	16	14	15	13
Nb	25.8	22.1	29.5	27.1	23.6	25.0	34.0	28.8	48.5	24.6	31.0	43.3	26.5
Ga	21	15	20	17	18	19	17	17	17	18	17	14	17
Cu	10	11	13	7	10	10	7	8	13	18	6	10	4
Zn	54	55	54	45	50	54	45	55	58	57	49	47	54
Pb	4	8	8	6	7	7	11	11	8	7	9	10	7
La	19	17	25	5	7	22	25	22	1	23	10	20	5
Ce	50	39	36	40	31	29	44	35	35	33	30	36	39
Th	4	5	4	7	5	5	9	5	3	6	4	6	5

Major elements are normalized on a volatile-free basis, with total Fe expressed as FeO.
"†" denotes values >120% of our highest standard.

Table 2: XRF geochemical data of 13 samples collected from the six deposits edupted from Glaicer Peak.

58
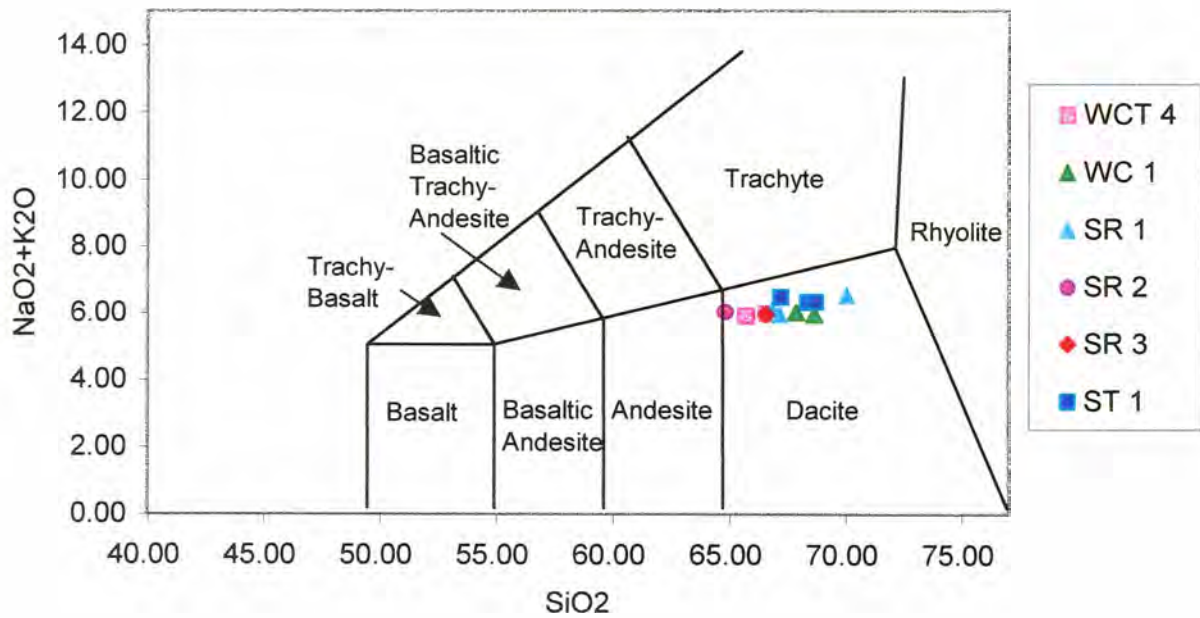
Figure 36. Total alkali versus silica (TAS) diagram showing the range of compositions of Glacier Peak deposits.
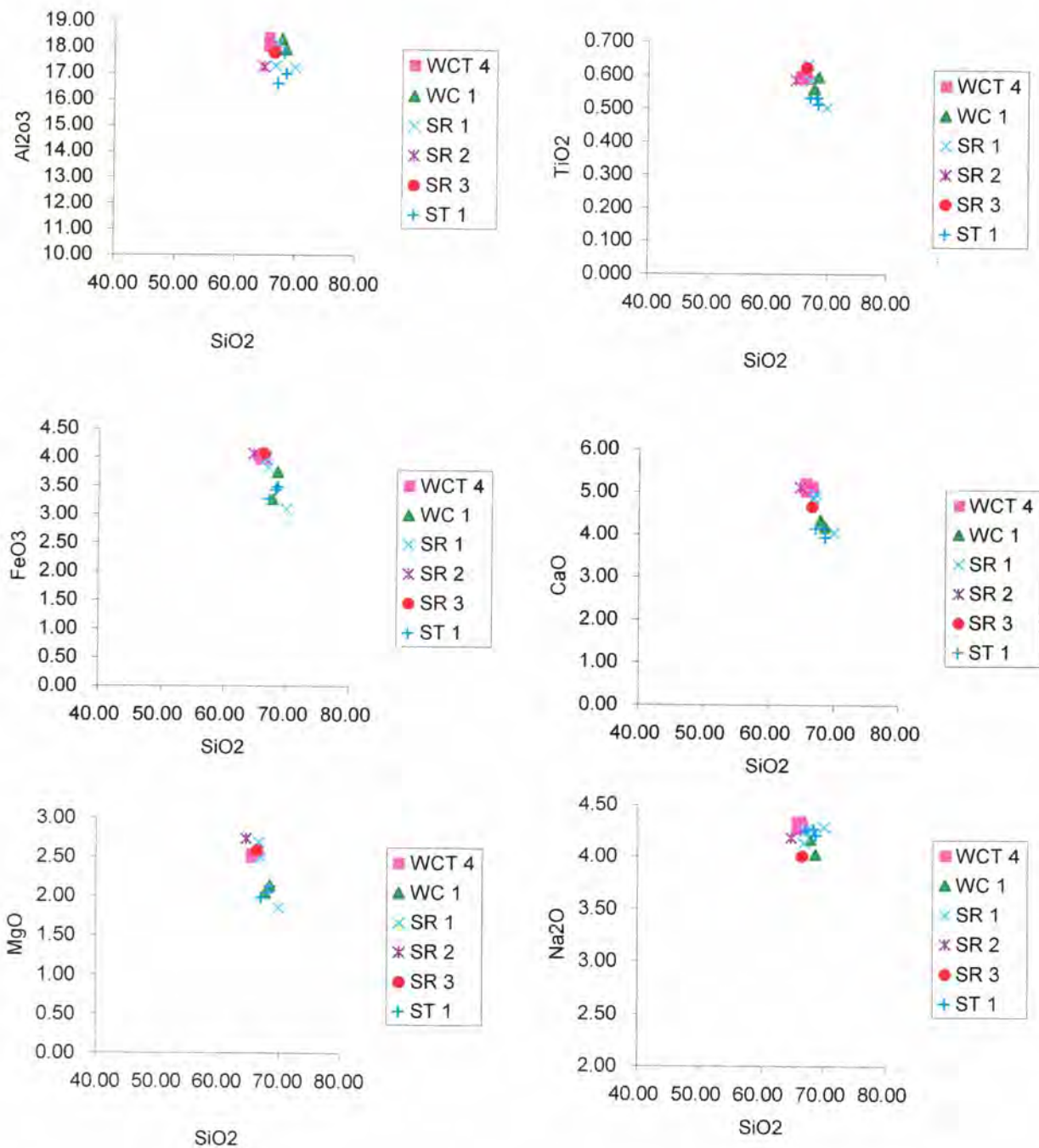
Figure 37. Major elements versus silica diagrams showing typical variations of evolving magma as silica increases, as occurs with the Glacier Peak deposits discussed in this study.
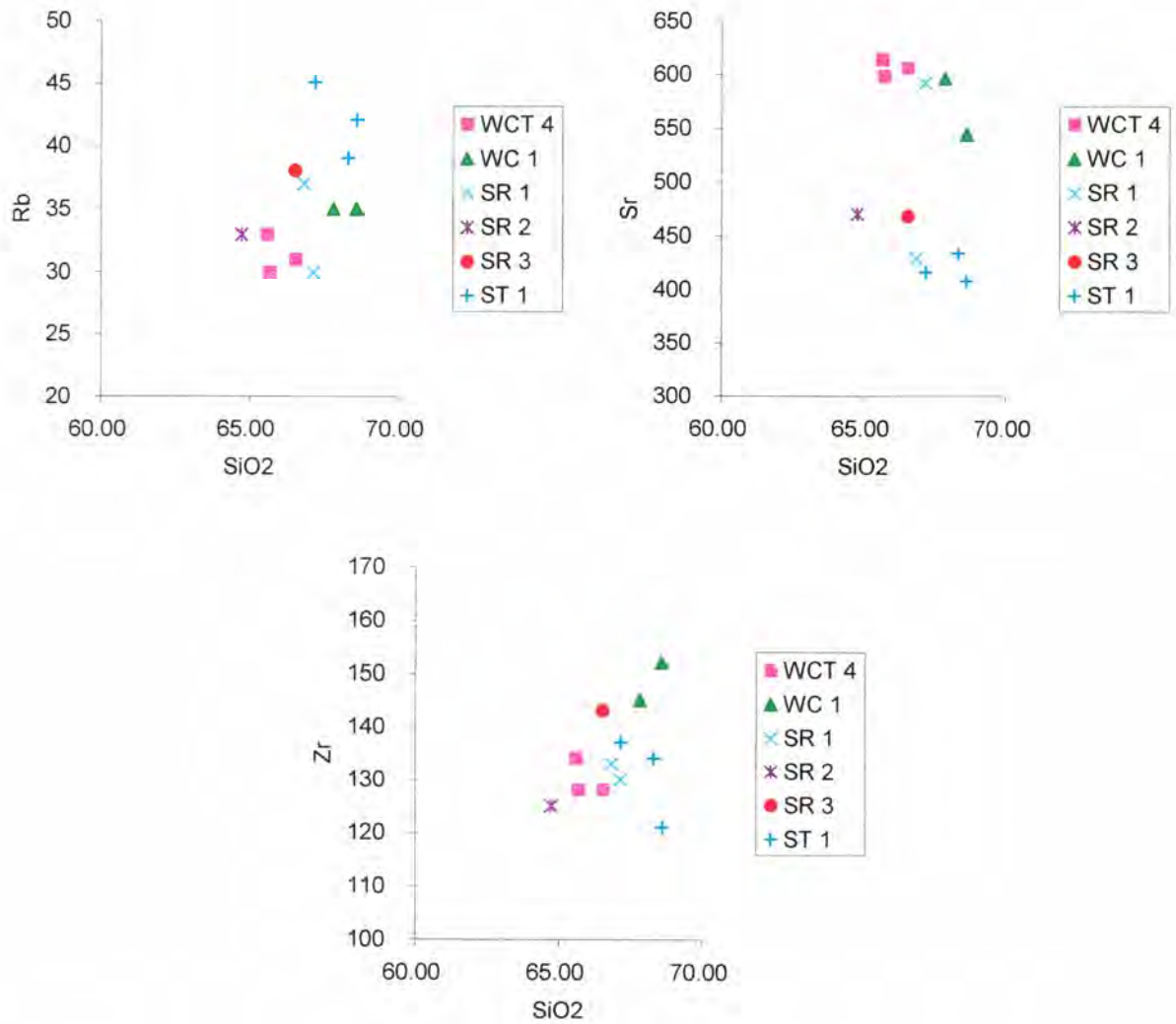
Figure 38. Variation of Rb, Sr, and Zr versus silica diagrams showing that Rb increases as silica increases and Sr decreases as silica increases in all deposits. The Glacier Peak post-glacial deposits do not overlap but are similar in trace element composition.

61
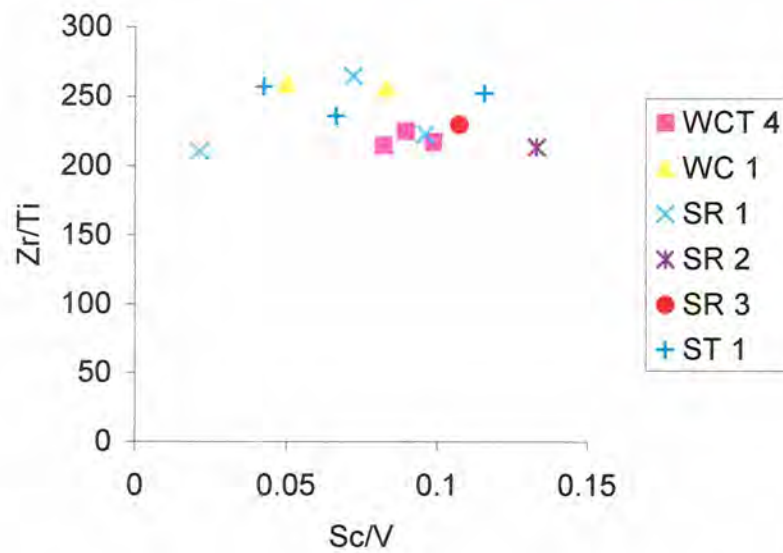
Figure 39. A variation diagram showing Zr/Ti versus Sc/V. The plot shows that the White Chuck Tuff samples are clustered and the distal deposit samples do not cluster amongst themselves nor do they cluster around the White Chuck Tuff samples.

Discussion

Mode of Emplacement

Anisotropy of Magnetic Susceptibility (AMS) techniques were used to determine the primary fabric and possible flow direction of the White Chuck Tuff and distal deposits. Figures 29 and 30 show the White Chuck tuff and distal deposit AMS axes respectively. The White Chuck Tuff and distal deposits differ considerably in that the orientations of the AMS axes are less well grouped in the distal deposits than in the White Chuck Tuff. This scatter of AMS axes in the distal deposits show that the orientation of individual clasts is independent of their internal fabric. Individual pumice clasts usually have an AMS lineation parallel to the stretched vesicles, demonstrating that an AMS lineation is developed before flow (Baer et al., 1997). While the individual pumiceous and non-vesicular clasts have magnetic fabrics, no preferential orientation of clasts is found within the same deposit, indicating that the AMS lineation in the clasts was developed before deposition. The White Chuck Tuff has an indurated groundmass, which has pumice clasts and lithic clasts. The magnetic fabric of the White Chuck Tuff sites has a well-defined orientation, consistent with its development during or after emplacement.

AMS fabrics of the White Chuck Tuff consistently have minimum axes that are steeply inclined and have oblate ellipsoid shapes (Figures 28 and 29). This is typical of AMS fabrics in tuff deposits (Tarling and Hrouda, 1993; Pennec et al., 1998; and Wolf et al., 1989). Fiamme or strained pumice clasts, evidence of post depositional settlement or rheomorphism, is not seen in the field; therefore the fabric of the White Chuck Tuff is

considered primary. In contrast the magnetic fabrics in post-depositional strained tuffs (Wolf et al. 1989 and Ellwood, 1982) are initially oblate and horizontal. Compaction and rheomorphism typically produce a prolate fabric (Pennec et al, 1998, Ellwood, 1982). The oblate and subhorizontal fabric in the White Chuck Tuff show that some settling has taken place during deposition, however rheomorphism has not occurred.

The magnetic foliation planes of ignimbrites usually show imbrication relative to the flow direction. The lineations also tend to be variable, being either parallel or perpendicular to the flow direction. Usually flow directions are characterized using the basal layers of ignimbrites (Baer et al., 1997). The White Chuck Tuff was sampled from the middle to upper levels of the flow. More chaotic depositional behavior probably occurs near the base where the flow is erosive, and in the upper levels where the flow may not be laminar.

AMS fabrics seen in the White Chuck Tuff sites suggest slight imbrication of the minimum axes. Imbrication, just as in sedimentary deposits, may reveal the flow direction of the tuff deposit. Confidence ellipses of the White Chuck Tuff were used to constrain the most likely foliation plane (Figure 29). The foliation plane defined by the mean of K_3 axis clearly dips southeast in White Chuck Tuff sites 1, 3, 4, 5, and 7. This is consistent with formation of mineral alignment due to imbrication of particles during deposition from a northwest traveling flow (Figure 12). The scatter of the K_1 axes in sites WCT-2 and WCT-6 is because they are located in the uppermost level of the deposit where chaotic non-laminar flow likely occurs.

Emplacement Temperature

The White Chuck Tuff, a Type I deposit, was deposited above the Curie temperature of magnetite (580° C). The paleomagnetic results show that when the White Chuck Tuff was deposited it exceeded 580° C. However the tuff was deposited below 800° C, the emplacement temperature at which ignimbrites weld (Cass and Wright, 1989).

The distal deposits have two component NRM demagnetization paths. The high-temperature component is more scattered and the low-temperature component is better clustered in deposits WC-1, SR-3, and ST-1, whereas SR-1, and SR-2 have equally scattered low temperature components at the high unblocking temperature components. The magnetization of the high-temperature component is unblocked from approximately 200°C to 300°C, in distal sites SR-1, SR-2, SR-3, and ST-1 (Figure 16). These unblocking temperatures are cooler then the 440°C Curie temperature of these same samples. This suggests that these distal sites are Type II deposits and could have been deposited at temperatures between ambient temperature and approximately 300°C. According to viscous magnetization results, the unblocking temperatures of these distal deposits were highly susceptible to a viscous remagnetization, so emplacement at ambient temperature is the most likely interpretation.

Distal deposit WC-1 has a low unblocking temperature at approximately 375°C, warmer than the other distal sites unblocking temperatures. WC-1 appears to be a Type III deposit and deposited at approximately 375°C.

The distal deposits appear to have originated from pyroclastic material. However the distal deposits were deposited at a warm temperature and are considered to be

unconsolidated pumice rich lahar deposits that cooled during transport down the White Chuck and Sauk River Valleys.

Paleomagnetic Relationships

Paleomagnetic site means of the White Chuck Tuff and distal deposits are plotted together on an equal area plot in Figure 40. The seven sites (circles) of the White Chuck Tuff indicate that the magnetic field was similar at each site when the sites were magnetized, which may indicate one or more sites originating from a single eruptive event. The five distal deposit site means are not grouped around the White Chuck Tuff site means. The distal deposits WC-1, SR-1, and ST-1 circles of 95% confidence of the low unblocking temperature component encompass the White Chuck Tuff site means. These distal deposits could share the White Chuck Tuff direction. The deposit SR-1 contains rip-up clasts of the White Chuck Tuff. The event that produced the SR-1 deposit occurred following the deposition of the White Chuck Tuff, but whether or not it is from the same eruptive event, is unknown. ST-1 has an imprecise site mean but shares the White Chuck Tuff direction. The site means of SR-2 and SR-3 do not plot near the other sites; therefore they are not part of the White Chuck Tuff. The large uncertainty of the distal site means is because the distal deposits cooled below the Curie temperature during transport and they have a high susceptibility to viscous remagnetization due to the abundance of low coercivity magnetic grains (Figure 27).

The low unblocking temperature component in the vesicular sample was highly susceptible to viscous remagnetization. The viscous remagnetization data in Figure 41 imply that there is a change in remanence over a short time with these samples. Samples

from the White Chuck Tuff did not show significant viscous properties. This does not disprove that viscous remagnetization had no effect on the White Chuck Tuff.
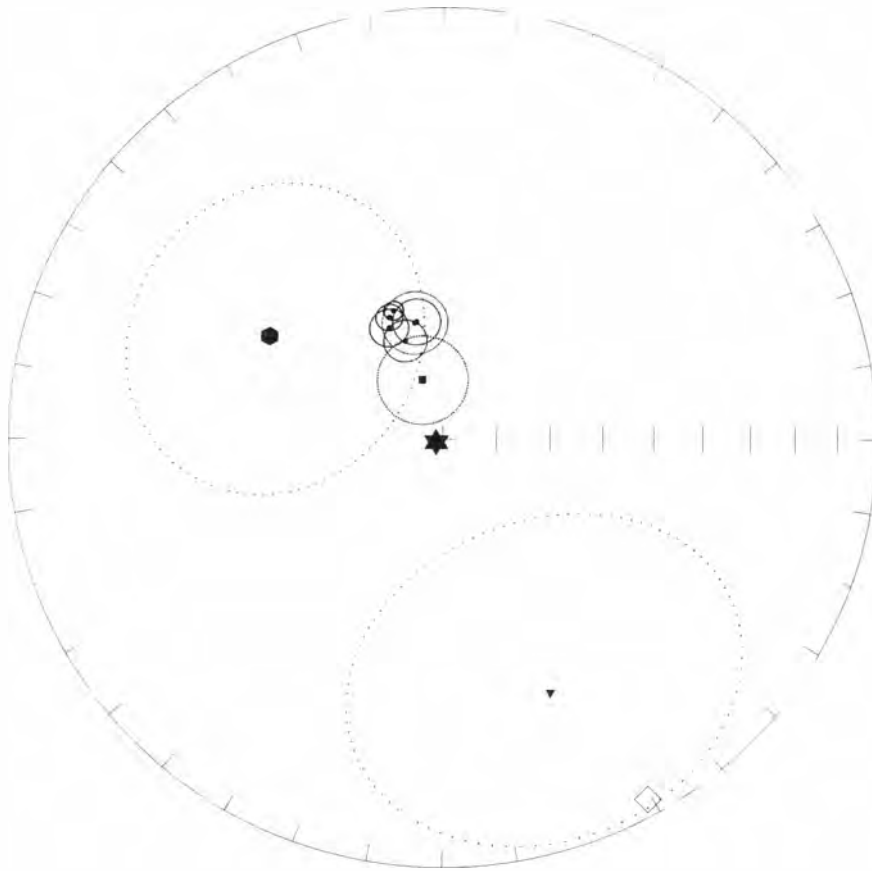
Figure 40. The distribution of the White Chuck Tuff and distal deposit site means on an equal area plot; WCT-1 - WCT-7 (circles), WC-1 (square), SR-1 (hexagon), SR-2 (diamond), SR-3 (triangle), and ST-1 (star). The circles of confidence are at the 95% confidence level. SR-2 and ST-1 site means were imprecise, therefore the 95% confidence circles were not used (Table 2). Although the ST-1 site mean could share the White Chuck Tuff direction, the site mean of SR-2 might not. (Tauxe, 1999)
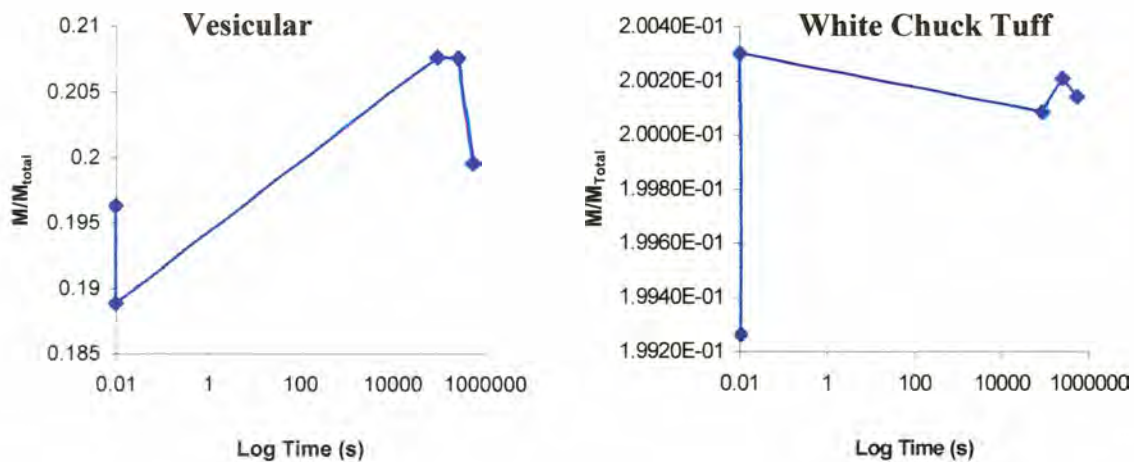
Figure 41. Viscosity tests of a vesicular sample from ST-1 (left) and a tuff sample from WCT-4 (right). The change in remanence over 5×10^5 seconds is significant in the vesicular specimen but not so much in the tuff. The samples had opposite behaviors during the test. The vesicular sample lost intensity, indicated by the vertical line at 0.01 log, while it was in the near zero magnetic field. Once the samples were placed in the Earth's magnetic field the magnetic intensity of the sample peaked and then progressively lost intensity towards its original field intensity. The tuff sample initially gained intensity during storage and lost intensity while back in the Earth's magnetic field.

The paleomagnetic direction of the tuff is close to the present day geomagnetic field. The tuff has a range of coercivities (Figure 21); therefore it will acquire viscous magnetization at different rates corresponding to particular coercivities and relaxation times. The low temperature demagnetization steps of the tuff, for example in Figure 16, did not result in large decay of remanence, indicating multi-domain magnetic minerals are not abundant. The viscosity test conducted in the lab is evidence that the high unblocking temperature directions are primary to the White Chuck Tuff.

Figure 42 displays relaxation time versus temperature for single domain and multi domain magnetites according to the single domain theory (Pulliah et al. 1975). The White Chuck Assemblage and Kennedy Creek Assemblage first-removed component's unblocking temperature and approximate relaxation time are plotted on the diagram with a red star and green star respectively. The unblocking temperatures were estimated by the time duration that a specimen was subjected to a particular temperature step, approximately 20 minutes. Figure 42 shows that the high unblocking temperatures of the White Chuck Tuff specimens are not likely to be viscous remagnetization due to the geomagnetic field in either the White Chuck Assemblage or Kennedy Creek Assemblage times. However the distal deposit specimens, with abundant low coercivity magnetic grains, are likely influenced by viscous remagnetization in the low unblocking temperature range for both assemblages. The unblocking temperatures of the distal deposits, Table 1, SR-2, SR-3 and ST-1 are the same as or below the estimated unblocking temperature for the complete removal of a viscous overprint produced at ambient temperature for approximately 10,000 years. Figure 42 also shows that at the
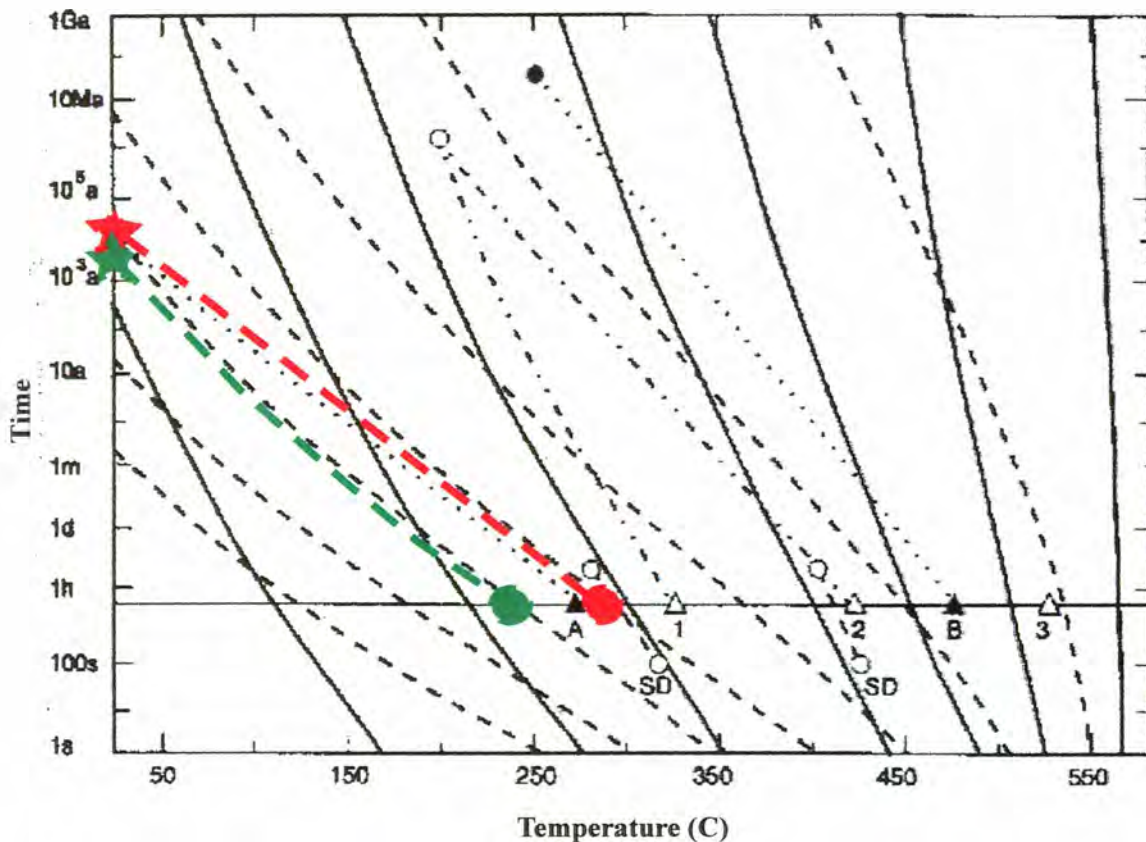
Figure 42. Single-domain and mixed single-domain/multi-domain blocking/unblocking time-temperature contours according to Pullaiah et al. (1975) (solid curves) and Walton (1980) (dashed curves) respectively. Each contour joins t and T values for which a particular ensemble of magnetic grains are just blocked (remagnetized) or unblocked (thermally demagnetized). Solid and open circles and triangles are geological and laboratory examples of low-temperature and high-temperature viscous overprints identifying the validity of the two sets of contours. The solid horizontal line marks approximately a 20-30 minute time range. This is the amount of time a sample may remain at a temperature step to remove the estimated viscous remanent magnetization. This was the time used in experiments by (Dunlop and Ozdemir, 1993) and in the analysis of this study. The red star and stippled line represent the White Chuck Assemblage deposits with SD and SD/MD ensembles. The estimated temperature at which the viscous overprint in a White Chuck Assemblage deposit should be removed is 300 C, and any unblocking temperatures above 300 C is primary remanence. The Green star represents samples from the Kennedy Creek Assemblage for reference to the younger deposits of Glacier Peak. If the deposits represented in this study originated from theKennedy Creek Assemblage deposits, viscous remagnetization may be observed as the low unblocking temperature component.
(Redrawn from Dunlop and Ozdemir, 1997)

71

unblocking temperatures for viscous remagnetization of distal younger deposits (~5,000 years old) at ambient temperature are possible. Distal deposits with higher unblocking temperatures, WC-1 and SR-1 (Table 1) may have the viscous overprint fully removed. The resultant low unblocking temperature did not appear to be viscous in origin due to their relatively linear demagnetization paths, MAD < 15, after using the low temperature treatment on distal deposit specimens.

Distal deposit sites SR-1, SR-2, SR-3, and ST-1 have two component NRMs with many scattered directions in both the low unblocking temperature and high unblocking temperature components (Figure 23). The scattered low unblocking temperature components in the most distal deposits most likely indicate Type II deposits because of scatter and the multiple reversed polarity directions in the low unblocking temperature range. The more well grouped specimens in the low unblocking temperature range have Type III characteristics but due to viscous effects this does not necessarily imply elevated emplacement temperature. The reversed polarity directions in the low unblocking temperature range in distal deposits SR-1 and SR-2 appear to have previous depositional histories associated with them and these clasts were not remagnetized during the last transport and deposition. The clasts that show this behavior were the nonvesicular clasts. The vesicular clasts were more clustered and showed the two component NRM was due to transport and deposition. Distal site WC-1, containing all vesicular samples, has a more well grouped low unblocking temperature component compared to the high unblocking temperature component. WC-1 is the only distal site that closely relates to a true Type III deposit (Hoblitt and Kellogg, 1978).

72

The White Chuck Tuff high unblocking temperature and distal deposit WC-1 low temperature site mean directions were used to calculate their corresponding Virtual Geomagnetic Poles (VGP) (Table 1). The VGPs of the deposits were compared to VGPs of a western North America paleosecular variation (PSV) curve (Hagstrum and Champion, 2002). Figures 43 and 44 shows the White Chuck Tuff and distal deposit WC-1 in pole space and their corresponding ages. The VGP from the White Chuck Tuff, previously believed to be ~11,670±250 b.p., does not fall near the secular variation curve from ~10,500 to 11,950 years b.p (Figure 43). However it does correspond with the VGP pole for 12,700 b.p. This is pole corresponds with the age of Tephra layer G of Glacier Peak 12,750 b.p. (Porter, 1978). In more recent research, Beget (1985) suggests that Tephra layer G was erupted later approximately 11,500 b.p., much later then previously thought. If the White Chuck Tuff does match the 12,700 year pole for Western North America then Tephra layer G could be 12,700 years old and related to the tuff.

The distal deposit WC-1 VGP is the only distal deposit that had sufficiently well defined low unblocking temperature components and site mean for comparison with the paleosecular variation data of Hagstrum and Champion (2002) (Table 1). WC-1 VGP datum is consistent with deposition between the time period of the White Chuck Assemblage and the Kennedy Creek eruptive period, approximately 9,180 years b.p., later then previously estimated (Figure 43). The WC-1 VGP circle of confidence does not overlap any of the VGPs of Hagstrum and Champion (2002) during the Kennedy Creek Assemplage time interval (Figure 44).

Figure 43. Virtual geomagnetic pole (VGP) postions
with a95 confidence limits from Hagstrum
and Champion (2002). VGPs of the White
Chuck Tuff and distal deposit WC-1 are plotted
amongst the western North American VGP
positions as listed in Table 1.
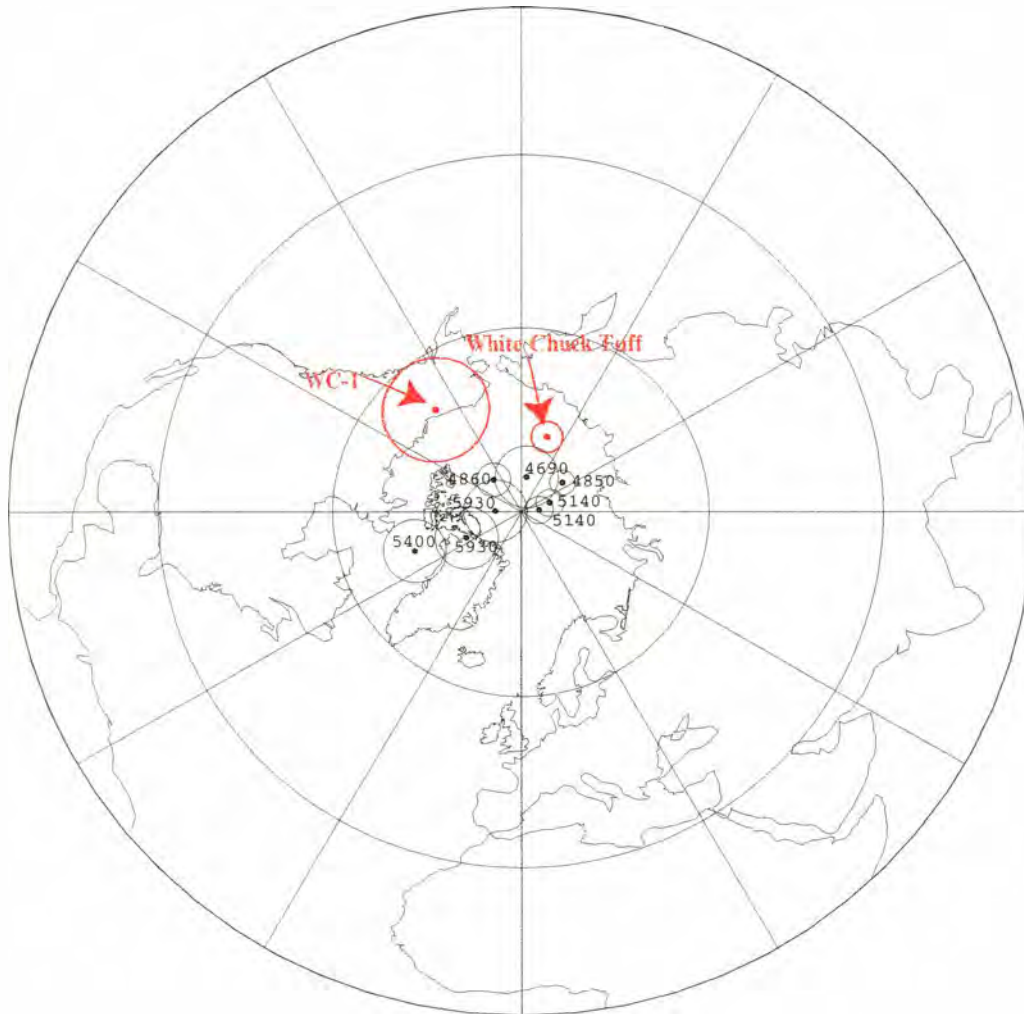
Figure 44. Virtual geomagnetic pole (VGP) postions
with a95 confidence limits from Hagstrum
and Champion (2002). VGPs of the White
Chuck Tuff and distal deposit WC-1 are plotted
amongst the western North American VGP
positions as listed in Table 1.

Mineralogical and Chemical Relationships

The petrography results indicate subtle differences between the White Chuck Tuff and the distal deposits (Figure 31). Mineralogical constituents of all deposits are the same except for SR-2, which contains oxyhornblende instead of hornblende. The differences between deposits are the abundance of minerals observed in thin section. The sites that are similar to the White Chuck tuff are SR-1 and SR-3. The sites WC-1 and ST-1 have similar mineralogy but the abundance of mafic minerals is greater in these sites.

Figure 37 shows typical trends of major elements versus silica of intermediate magma compositions and indicate Glacier Peak magma evolved by fractionation. However trace element diagrams indicate that White Chuck Tuff and distal deposits are not dissimilar chemically (Figure 38). There is no consistent overlap or difference between deposits in the trace element diagrams or the variation diagram, Figure 39. The chemistry of the distal deposits does not indicate whether they are related to the White Chuck Tuff.

Conclusions

Anisotropy of magnetic susceptibility, paleomagnetism, petrography, and chemistry were used to characterize Glacier Peak proximal and distal pyroclastic deposits, in particular the White Chuck Tuff and five distal deposits greater than 30 km west of Glacier Peak. Distal deposits may hold the clues to the correlation of the proximal White Chuck Tuff to unconsolidated runout deposits. The following conclusions characterize the White Chuck Tuff and distal deposits.

1. The indurated White Chuck Tuff was deposited during one event. All samples of the tuff are similar in paleomagnetism, petrography, and chemistry. Debris of the White Chuck Tuff traveled westward down the White Chuck River Valley and was emplaced at temperatures above 580°C and below 800°C.

2. The AMS measurements of the White Chuck Tuff indicate an overall northwestward downvalley flow direction. The distal deposits AMS fabrics had no consistent orientation. This was due to the magnetic fabric being formed in individual clasts prior to deposition.

3. The first removed component of remanence of the distal deposits has unblocking temperatures that decrease westward, in the apparent direction of transport. However, only one site (WC-1) has clustered magnetization directions for both first and second removed components. This indicates WC-1 is a Type III deposit, emplaced at a temperature as high as 350° C. The other distal deposits have scattered

directions indicating that they were products of cooler lahars at ambient temperature that traveled down the White Chuck River Valley.

4. The paleomagnetic direction of the White Chuck Tuff is well defined with a mean declination of 342° and inclination of 60°. The White Chuck Tuff is within the 95% circles of confidence of distal deposit site means WC-1, SR-1, and ST-1. Deposits SR-2 and SR-3 site means do not plot near the White Chuck Tuff mean.

5. Viscous remagnetization may affect vesicular samples of the distal deposits SR-1, SR-2, SR-3, and ST-1, but the two component NRM and upward low unblocking temperature directions show that the clasts of the distal deposits were emplaced as Type II deposits. These deposits were deposited below the Curie temperature of both the non-vesicular and vesicular clasts magnetic minerals. These contributed to the uncertainty of site mean directions of the distal deposits.

6. The White Chuck Tuff and distal deposits all fall in the dacite field explaining the explosive nature of the eruptions. The overall chemical variations of Glacier Peak deposits indicate typical intermediate magma compositional trends. However, these variations of the White Chuck Tuff and the distal deposits do not have consistent similarities or differences, and show no conclusive evidence that the distal deposits are related to the White Chuck Tuff.

7. Paleomagnetism does not support the assumed age of approximately 11,500 years ago, for the White Chuck Tuff. Instead it supports

deposition towards the beginning of the White Chuck Assemblage eruptive cycle. The virtual geomagnetic poles of the White Chuck Tuff deposit correspond with the 12,750 b.p. VGP of Hagstrum and Champion (2002). 12,750 b.p. also corresponds to a major eruption of Glacier Peak that produced the deposit Tephra G.

8.   The VGP of distal deposit WC-1 corresponds with the 9180 +290/-200 b.p. VGP (Hagstrum and Champion, 2002) towards the end of the Kennedy Creek eruptive cycle. Other distal deposits VGPs are not well enough defined to be useful, but from field relationships associated with the deposition and location of other deposits, they were erupted during the Kennedy Creek Assemblage.

9.   Glacier Peak has produced hot material that traveled down the White Chuck River Valley, displayed in the White Chuck Tuff and distal deposit WC-1. The White Chuck Tuff was deposited at a minimum temperature of 580° C approximately 17 km west of Glacier Peak. Distal deposit WC-1 was deposited at a maximum temperature of approximately 375° C, which could be classified as a hot deposit (Cas and Wright, 1989). The material of WC-1 retained these elevated temperatures during transport to at least 30 km from Glacier Peak. Glacier Peak is capable of producing hot ash flows that travel great distances. The hazards associated with Glacier Peak have been known as ash deposits and lahars, and as seen from this study pyroclastics are recent and extensive products of Glacier Peak.

References

Akimoto, S., Nagata, T., Katsura, T., 1957, The $TiFe_2O_5$-$TiFeO_5$ solid solution series, Nature, vol. 179, no. 4549, pp. 37-38.

Aramaki, S., Akimoto, S., 1957, Temperature Estimation of Pyroclastic Deposits by Natural Remanent Magnetism, American Journal of Science, vol. 255, no. 9, pp. 619-627.

Bacon, C. R., Druitt, T. H., 1988, Compositional evolution of the zoned calcalkaline magma chamber of Mount Mazama, Crater Lake, Oregon, Contributions to Mineralogy and Petrology, vol. 98, pp. 224-256.

Baer, E. M., Fuller, M., Valentine, G., 1997, Turbulent Transport and Deposition of the Ito Pyroclastic Flow: Determinations using Anisotropy of Magnetic Susceptibility, Journal of Geophysical Research, vol. 102, no. B10, pp. 22,565-22,586.

Beget, J. E., 1981, Postglacial Volcanic Hazards at Glacier Peak, Washington: University of Washington Doctor of Philosophy Thesis, 192p.

Beget, J. E., 1981, Glacier Peak Volcano: Tephrochronology, Eruption History and Volcanic Hazards, Self, S. and Sparks, R. S. J. editors, Tephra Studies, D. Reidel Publishing Company, pp. 449-455.

Beget, J. E., 1981, Early Holocene glacier advance in the North Cascade Range, Washington, Geology, vol. 9, pp. 409-413.

Beget, J. E., 1982, Recent Volcanic Activity at Glacier Peak, Science, vol. 215, pp. 1389-1390.

Beget, J. E., 1983, Glacier Peak, Washington: A Potentially Hazardous Cascade Volcano, Environmental Geology, vol. 5, no. 2, pp. 83-92.

Beget, J. E., 1985, Tephrochronology of Late Wisconsin Deglaciation and Holocene Glacier Fluctuations near Glacier Peak North Cascade Range, Washington, Quaternary Research, vol. 21, pp. 304-316.

Beget, J. E., 1985, Tephrochronology of antislope scarps on an alpine ridge near Glacier peak, Washington, USA, Arctic and Alpine Research, vol. 17, no. 2, pp. 143-152.

Beget, J. E., 1990, Volcanoes of Washington: Glacier Peak, Washington, Wood, C. A., Kienle, Juergen, compilers and editors, Volcanoes of North America: United States and Canada, Cambridge University Press, New York, pp. 156-158.

Best, M. G. and Christiansen, E. C., 2001, Igneous Petrology, Blackwell Science, pp. 262-280.

Borradaile, G. J., 1994, Low-temperature demagnetization and ice-pressure demagnetization in magnetite and haematite, Geophysical Journal International, vol. 116, pp. 571-584.

Borradaile, G. J., Lagroix, F., and Trimble, D., 2001, Improved isolation of archeomagnetic signals by combined low temperature and alternating field demagnetization, Geophysical Journal International, vol. 147, pp. 176-182.

Butler, R. F., 1998, Paleomagnetism: Magnetic Domains to Geologic Terranes.

Cas, R. A. F., and Wright, J. V., 1987, Volcanic Successions Modern and Ancient, a geological approach to processes, products and successions, Allen & Unwin, London.

Collinson, D. W., 1983, Methods in Rock Magnetism and Paleomagnetism: Techniques and Instrumentation, Champman and Hall, London.

Dragovich, J. D., McKay, D. T. Jr., 2000, Holocene Glacier Peak Lahar Deposits in the Lower Skagit River Valley, Washington, Washington Geology, vol. 28, no. 1,2, pp. 19-21.

Dragovich, J.D, Gilbertson, L. A., Lingley, W. S., Plienz, M. Jr., Glenn, J, 2002, Geologic Map of the Fortson 7.5-minute Quadrangle, Skagit, and Snohomish Counties, Washington, Open File Report 2002-6.

Dragovich, J.D, Gilbertson, L. A., Lingley, W. S., Plienz, M. Jr., Glenn, J, 2002, Geologic Map of the Darrington 7.5-minute Quadrangle, Skagit, and Snohomish Counties, Washington, Open File Report 2002-7.

Dunlop, D. J., Ozdemir, O., 1993, Thermal Demagnetization of VRM and pTRM of single domain magnetite: No evidence for anomalously high unblocking temperatures, Geophysical Research Letters, vol. 20, no. 18, pp. 1939-1942.

Dunlop, D. J., Ozdemir, O., 1997, Rock Magnetism: Fundamentals and frontiers, Cambridge University Press, United Kingdom.

Ellwood, B. B., 1982, Estimates of flow direction for calc-alkaline welded tuffs and paleomagnetic data reliability from anisotropy of magnetic susceptibility measurements: central San Juan Mountains, southwest Colorado, Earth and Planetary Science Letters, vol. 59, pp. 303-314.

Enkin, R. J. and Dunlop, D. J., 1988, The demagnetization temperature necessary to remove viscous remanent magnetization, Geophysical Research Letters, vol. 15, no. 5, pp. 514-517.

Fisher, R. A., 1953, Dispersion on a sphere, Proc. Royal Society of London, Ser. A, vol. 217, pp. 295-305.

Fisher, R. V., Ort, O. F., Heiken, F., 1993, Mobility of a large-Volume Pyroclastic Flow-Emplacement of the Campanian Ignimbrite, Italy, Journal of Volcanology and Geothermal research, vol. 56, pp. 205-220.

Flinn, D., 1962, On folding during three-dimensional progressive deformation, Geological Society of London Quarterly Journal, vol. 118, pp. 385-433.
Foit, F. F., Mehringer, P. J., and Sheppard, J. C., Jr., 1993, Age Distribution and Stratigraphy of Glacier Peak Tephra in Eastern Washington and Western Montana, United States, Canadian Journal of Earth Sciences, vol. 30, pp. 535-552.

Ford, Authur Barnes, 1959, Geology and petrology, Glacier Peak Quadrangle, Northern Cascades, Doctoral Thesis, University of Washington.

Gardner, J. E., Carey, S., and Sigurdsson, H., 1998, Plinian Eruptions at Glacier Peak and Newberry Volcanoes, United States: Implications for Volcanic Hazards in the Cascade Range, GSA Bulletin, vol. 110, no. 2, pp. 173-187.

Hagstrum, J. T., Champion, D. E., 2002, A Holocene paleosecular variation record from ^{14}C-dated volcanic rocks in western North America, Journal of Geophysical Research, vol. 107, mo. B1, pp. 1-14.

Heki, K., 1983, Paleomagnetic Study of the Higashi-Izu Monogenetic Volcano Group and Pyroclastic Flow Deposits in Dagoshima Prefecture: Paleosecular Variation during the Last 40,000 years in Japan, Journal of Geomagnetism and Geoelectricity, vol. 35, pp. 383-390.

Hildreth, W., Mahood, G., 1985, Correlation of ash-flow tuffs, Geological Society of America Bulletin, vol. 96, pp. 968-974.

Hoblitt, R. P., Kellogg, K. S., 1979, Emplacement temperatures of unsorted and unstratified deposits of volcanic rock debris as determined by paleomagnetic techniques, Geological Society of America Bulletin, vol. 90, pp. 633-642.

Hoblitt, R. P., Miller, C. D., and Scott, W. E., 1987, Volcanic Hazards with regard to Siting Nuclear-Power Plants in the Pacific Northwest: USGS Open-File Report 87-297.

Hoblitt, R. P., Reynolds, R. L., Larson, E. E., 1985, Suitability of nonwelded pyroclastic-flow deposits for studies of magnetic secular variation: A test based on deposits emplaced at Mount St. Helens, Washington, in 1980, Geology, vol. 13, pp. 242-245.

Jackson, M., William, G., Marvin, J., and Banerjee, S. K., 1988, Partial anhysteretic remanence and its anisotropy: applications and grainsize-dependence, Geophysical research letters, vol. 15, no. 5, pp. 440-443.

Kelso, P. R. and Banerjee, S. K., 1994, Elevated temperature viscous remanent magnetization of natural and synthetic multidomain magnetite, Earth and planetary Science Letters, vol. 22, pp. 43-56.

Kent, D. V., Ninkovich, D., Pescatore, T., Sparks, S. R. J., 1981, Palaeomagnetic determination of emplacement temperature of Vesuvius AD 79 pyroclastic deposits, Nature, vol. 290, pp393-396.

Levy, S. S., and O'Neil, J. R., 1989, Moderate-temperature zeolitic alteration in a cooling pyroclastic deposit, Chemical Geology, vol. 76, pp. 321-326.

Kruiver P. P., Dekkers, M. J., Heslop, D., 2001, Quantification of magnetic coercivity components by the analysis of acquisition curves of isothermal remanent magnetization, Earth and Planetary Science Letters, vol. 189, pp. 269-276.

Lowrie, W., 1990, Identification of Ferromagnetic Minerals in a Rock By Coercivity and Unblocking Temperature Properties, Geophysical Research Letters, vol. 17, no. 2, pp. 159-162.

McElhinny, M. W. and McFadden, P. L., 2000, Paleomagnetism: Continents and Oceans, Academic Press, 2nd Edition.

Mandeville, C. W., Carey, S., Sigurdsson, H., King, J., 1994, Paleomagnetic evidence for high-temperature emplacement of the 1883 subaqueous pyroclastic flows from Krakatau Volcano, Indonesia, Journal of Geophysical Research, vol. 99, no. B5, pp. 9487-9504.

Major, J. J. and Newhall, C., 1989, snow and ice perturbation during historical volcanic eruptions and the formation of lahars and floods, Bulletin of Volcanology, vol. 52, no. 1, pp. 1-27.

Mastin, L. G., and Waitt, R. B., 1995, Is Glacier Peak a Dangerous Volcano?: USGS Open-File Report 95-413.

Mastin, L. and Waitt, R., 2000, Glacier Peak – History and Hazards of a Cascade Volcano, USGS Fact Sheet, 058-00.

Nagata, T., 1961, Rock Magnetism, Maruzen Company LTD., Tokyo.

Naranjo, J. L., Sigurdsson, H., Carey, S. N., Fritz, W., 1986, Eruption of the Nevado Del Ruiz Volcano, Colombia, on 13 November 1985: Tephra Fall and Lahars, Science, vol. 233, pp. 961-963.

Ohno, M. and Hamano, Y., 1992, Geomagnetic poles over the past 10,000 years, Geophysical Research Letters, vol. 19, no. 16, pp. 1715-1718.

Smith, Henry W., and Okazaki, Rose, 1977, Electron Microprobe Data for Tephra Attributed to Glacier Peak, Washington, Quaternary Research, vol. 7, pp. 197-206.

O'Reilly, W., 1984, Rock and Mineral Magnetism, Blackie, Glasgow and London.

Pennec, J. Le, Chen, Y., Diot, H., Froger, J., Gourgaud, A., 1998, Interpretation of anisotropy of magnetic susceptibility fabric of ignimbrites in terms of kinematic and sedimentological mechanisms: An Anatolian case-study, Earth and Planetary Science Letters, vol. 157, pp. 105-127.

Porter, S. C., 1978, Glacier Peak Tephra in the North Cascade Range, Washington: Stratigraphy, Distribution, and Relationship to Late-Glacial Events, Quaternary Research, vol. 10, no. 1, pp. 30-41.

Pullaiah, G., Irving, E., Buchan, K. L., and Dunlop, D. J., 1975, Magnetization changes caused by burial and uplift, Earth and planetary Science Letters, vol. 28, pp. 133-143.

Riddihough, Robin P., 1984, Recent movements of the Juan de Fuca plate system, Journal of Geophysical Research B, vol. 89, no. 8, pp. 6980-6994

Sporer, H., 1984, On viscous remanent magnetization of synthetic multidomain titanomagnetite, Geophysical research letters, vol. 11, no. 3, pp. 209-212.

Su, Yongjun, Langmuir, Charles H., Asimow, Paul D., 2003, PetroPlot, a plotting and data management tool set for Microsoft Excel, Geochemistry, Geophysics, Geosystems – G (super 3), vol. 4, no. 3, pp. 14

Tabor, R. W. and Crowder, D. F., 1969, Batholiths and Volcanoes- Intrusion and eruption of Late Cenozoic Magmas in the Glacier Peak Area North Cascades, Washington, U.S. Geological Survey Professional Paper 604.

Talor, Dylan D., 2001, Petrology and Geochemistry of Mafic Lavas Near Glacier Peak, North Cascades, Washington, Master Thesis, Western Washington University, pp. 90.

Tarling, D. H., Hrouda, F., 1993, The Magnetic Anisotropy of Rocks, Chapman and Hall, London.

Tauxe, L, 1999, Paleomagnetic Principles and Practices, Kluwer Academic Publishers, Boston.

Tivey, M. and Johnson, P. H., 1981, Characterization of viscous remanent magnetization in single- and multi-domain magnetite grains, Geophysical Research Letters, vol. 8, no. 3, pp. 217-220.

Tivey, M. and Johnson, P. H., 1984, The Characterization of viscous remanent magnetization in Large and Small Magnetite particles, Journal of geophysical research, vol. 89, no. B1, pp. 543-552.

Torii, M., Dharma, A., and Takuo, Y., 1982, Thermal Demagnetization Experiments of Welded Tuff, Sigura-Gura Formation, Sumatra, Indonesia, Rock Magnetism and Paleogeophysics, vol. 9, pp. 1-3.

Vance, J. A., 1957, The Geology of the Sauk River Area in the Northern Cascades of Washington, University of Washington Dissertation, 312 pp.

Waitt, R. B., Mastin, L. G., and Beget, J. E., 1995, Volcanic-Hazard Zonation for Glacier Peak Volcano, Washington, USGS Open-File Report 95-499.

Walton, D., 1980, Time-temperature relations in the magnetization of assemblies of single domain grains, Nature, vol. 286, pp. 245-247.

Walton, D., 1983, Viscous magnetization, Nature, vol. 305, pp. 616-619.

Westgate, J. A., Evans, M. E., 1978, Compositional Variability of Glacier Peak tephra and its Stratigraphic Significance, Canadian Journal of Earth Sciences, vol. 15, pp. 1554-1567.

Wilson, C. J. N., Hildreth, W., 1997, The Bishop Tuff: New Insights from Eruptive Stratigraphy, Journal of Geology, vol. 105, pp. 407-439.

Wilson, C. J. N., and Houghton, B. F., 2000, Pyroclast transport and deposition, Encyclopedia of Volcanoes, Academic Press, pp. 545-553.

Wilson, C. J. N., Houghton, B. F., Kamp, P. J. J., and McWIlliams, M. O., 1995, An exceptionally widespread ignimbrite with implications for pyroclastic flow emplacement, Nature, vol. 378, pp. 605-607.

Wilson, C. J. N., and Walker, G. P. L., 1982, Ignimbrite depositional facies: the anatomy of a pyroclastic flow, Journal of the Geological Society of London, vol. 139, pp. 581-592.

Wolff, J. A., Ellwood, B. B., Sachs, S. D., 1989, Anisotropy of magnetic susceptibility in welded tuffs: application to a welded-tuff dyke in the Tertiary Trans-Pecos Texas volcanic province, USA, Bulletin of Volcanology, vol. 51, pp. 299-310.

Zlotnicki, J., Pozzi, J. P., Boudon, G., Moreau, M. G., 1984, A new method for the determination of the setting temperature of pyroclastic deposits (example of Guadeloupe: French West Indies), Journal of Volcanology and Geothermal Research, vol. 21, pp. 297-312.

Appendix I

Sample site locations and descriptions

Appendix 1a.1-7. A landslide scar exposes the White Chuck Tuff and 2000 cm of hillside on the north side of the White Chuck River trail at N48 W121, Glacier Peak Quadrangle. The stratagraphic section below represents sites WCT-1 through WCT-7. Descriptions of stratigraphy above and below the White Chuck Tuff may be referenced to Beget, 1981. (Figure 4)

Thickness (cm)

Colluvium: reworked ash and forest duff..32

Tephra layer..10-20

Forest duff: Contains fragments of burned branches............................10-50

Reworked fluvial sand and gravel, interbedded with thin lahars that contain blocks of White Chuck Tuff up to 1 m in diameter..300

Lahar: Subangular to subrounded cobbles and boulders up to 50 cm in diameter in matrix of sand and silt; no apparent sorting or stratification; contains reworked blocks of the vitric tuff...400

White Chuck Tuff: Pyroclastic flow deposit, indurated, with well-developed columnar jointing, columns average 1-2 m in diameter; deposits form prominent cliff in outcrop; contains abundant unflattened pumice lapilli (sampled)................................800

Pyroclastic deposits: at least 10 pyroclastic flow deposits; mostly light gray; pumiceous ashy matrix, non-vesicular rock fragments mostly light-gray dacite, with some white to medium-gray pumice; some deposits are reversely graded; some contain boulders as large as 1 m in diameter; prismatically jointed boulders common..........................≤2500

87

Appendix 1b. Site WC-1 is located at N48.1 W121.27 about 0.5 miles from the beginning of the Mountain Loop Highway, White Chuck Mountain quadrangle. The description of unstudied deposits are referenced from Beget, 1981.

Thickness (cm)

Alluvium, thin sand and silt beds, horizontally stratified and interbedded with pumiceous lahars; contains blocks as much as 30 cm in diameter of the White Chuck Tuff........60

Lahar: Sandy-silty matrix; no apparent sorting of or stratification; contains rare blocks of White Chuck Tuff..20

Pyroclastic: Pumiceous clasts in silty-sand ash matrix; reversely graded; contains white gray pumice lapilli; there are circular voids that appear to have been tree logs, which were described as visible and sampled by Beget, 1981 and described as correlative with the White Chuck Tuff. (Sampled as WC-1)..10-30

Silty alluvium: cross-bedded; crystal-rich fine ash......................................10

Lahar: pumice lapilli in fine sand matrix; light gray......................................10

Lahar: Pumice lapilli in fine sand matrix; light gray to gray..............................30

Site WC-1 showing the unconsolidated pyroclastic deposits sampled

Appendix 1c. Site SR-1 is located approximately 2.5 km south of Darrington at N48.14 W121.35, Darrington quadrangle.

Thickness (cm)

Lahar: Sandy-silty groundmass; no apparent sorting of or stratification; contains rare blocks of White Chuck Tuff...200

Lahar: pumice lapilli and dacite clasts in fine dacitic sand groundmass; light gray with occasional ripup clasts of the White Chuck Tuff (sampled as SR-1)............150

Alluvium: Dacite clasts and exotic boulders approximately 30-90 cm in diameter in a silty sand groundmass; gray to light brown...100

Silty alluvium: cross-bedded; crystal-rich fine ash and exotic medium to coarse sand; light brown...50

Site SR-1 showing pumiceous clasts entrained in the groundmass. These clasts were sampled for this study

Site SR-1 photo showing large boulders were transported by a pyroclastic flow 40 km from Glacier Peak.

Appendix 1d: Site SR-2 is located approximately 5 km North of Darrington at N48.17 W121.33 on private property just above the present Sauk River flood plain, Darrington Quadrangle.

Thickness (cm)

Lahar: Sandy-silty groundmass; no apparent sorting of or stratification; contains rare blocks of White Chuck Tuff...200

Lahar: pumice lapilli and dacite clasts in fine dacitic sand groundmass; light gray (sampled as SR-2)..150

Appendix 1e: Site SR-3 is located at the intersection of WA. Hwy. 530 and the Sauk-Prairie Road, N48.16 W121.36, Darrington Quadrangle.

Thickness (cm)

Lahar: pumice lapilli and dacite clasts in fine dacitic sand groundmass; light gray (sampled as SR-3)..200

Appendix 1f: Site ST-1 located along the North Fork Stillaguamish River Valley at N48.16 W121.38, approximately 3 km west of Darrington, Fortson Quadrangle. (Figure 9a)

Thickness (cm)

Alluvium: Horizontally stratified ashy sand and silt beds with dacite and exotic gravel and cobbles up to 30 cm in diameter...60

Lahar: Reversely graded and corss bedded pumice lapilli up to 17 cm in diameter in a ashy sandy groundmass...60

Pyroclastic: Pumice lapilli and dacite clasts in fine dacitic sand groundmass; light gray...150

Trphra: Consolidated crystal rich fine ash...6

Appendix II

Rock Magnetic Methods

Partial Anhysteretic Remanent Magnetization: Partial Anhysteretic Remanent Magnetization (pARM), a coercivity spectrum analysis (Buttler, 1998), was performed on specimens from different sites. A D-Tech D-2000 Alternating Field Demagnetizer with a DE coil was used to generate the pARM. Partial Anhysteretic Remanent Magnetization was used to understand the size distribution of magnetic grains in dacite and pumice clasts from Glacier Peak. The data may be plotted graphically to display the coercivity range of the most abundant magnetic minerals present in the sample, which provides information on their grainsize (Jackson et al, 1988).

Isothermal Remanent Magnetization: Exposing samples (usually at room temperature) to a magnetizing field (H) generated by an electromagnet creates Isothermal Remnant Magnetization (IRM) (Butler, 1998). Ferromagnetic grains with a coercive force less than the applied field acquires IRM. In the laboratory IRM is used as another form of coercivity spectrum analysis. The procedure is to expose a sample to a magnetic field, measure the resulting IRM, and then repeat the procedure using a stronger magnetizing field. A sample containing only titano-magnetite acquires IRM in a magnetic field ≤ 300 mT, but no additional IRM is acquired in higher magnetic fields. If other ferromagnetic minerals such as hematite are present in a sample, IRM is gradually acquired in H up to 3T.

Lowrie Method: The analytical method that has come to be known as the Lowrie method (Lowrie, 1990) is a combined method of IRM acquisition and progressive thermal demagnetization of the IRM. This method is used to interpret the ferromagnetic mineral content of a rock. The x-axis, y-axis, and z-axis of a specimen are given an IRM using different magnetic field strengths. Subsequent progressive thermal

demagnetization is able to identify minerals, which have similar maximum coercivities that generally have different characteristic unblocking temperatures, for example the unblocking temperature of magnetite is approximately 580° C. If magnetite dominates the magnetic mineralogy in a sample the demagnetization of the IRM will decay smoothly to zero by 580° C.

Curie Temperature: The Curie point is the temperature below which magnetic minerals in a rock can acquire a magnetization. The Curie temperature of individual clasts was measured using an AGICO KLY-3-s Magnetic Susceptibility Bridge and a CS-3 Furnace. The samples were crushed into powder and placed in a test tube with an alumina-spacing agent. The tube was placed in the furnace and the susceptibility was measured at incremental temperature steps to the target temperature 610° C. Curie temperatures may indicate differences in TiO_2 content in magnetite and oxide equilibration temperature by measuring a specimen's susceptibility at different temperatures. Two thermomagnetic curves are generated from the measurements, the heating curve and cooling curve. The Curie temperatures of clasts were estimated by using the intersection point of the two tangents to the thermomagnetic curve that bounds the Curie temperature.

Viscous Remanent Magnetization: Viscous Remanent Magnetization (VRM) is the gradual change of remanent magnetization in ferromagnetic substances over time during exposure to weak magnetic fields. The time-decay of the already acquired remanent magnetization, such as TRM, results in a secondary magnetization from the weak external geomagnetic field. This rate of decay is quantified by the relaxation time and is controlled by the volume and coercive force (Hc) of a magnetic grain. The inverse

relationship between these two properties allows acquisition of VRM to take place (low coercive force/high volume). In single domain grains, the acquisition of VRM is essentially the inverse of magnetic relaxation. The VRM is acquired by the realignment of magnetic moments of grains with short relaxation times.

After allowing four representative samples, 1 tuff, 1 non-vesicular, and 2 vesicular, to relax for four months in a low magnetic field, the samples were placed with the z-axis parallel to the present day measured geomagnetic field. Over the course of six 24-hour periods each sample's magnetization was measured documenting the relationship of time and magnetization acquired over the period of 144 hours.

Appendix III
Thin Section Point Counts

Sites	Thin Section Constituents and Points Counts								
	Matrix	Void	Feldspar	Hornblende	Hypersthene	Oxyhornblende	Clinoproxene	Opaque	Total
WCT-1	196	95	64	14	3	2	0	3	377
WCT-2	309	33	81	15	6	0	0	2	446
WCT-3	247	64	94	17	4	0	3	8	437
WCT-4	266	73	94	18	0	0	1	15	467
WCT-7	261	86	76	14	3	0	1	5	446
WC-1	376	31	131	14	11	0	5	12	580
SR-1	234	120	78	12	6	0	3	3	456
SR-2	255	119	133	0	13	4	3	10	537
SR-3	247	83	128	24	5	0	2	4	493
ST-1	200	42	57	9	1	0	1	2	312

Thin section point counts of minerals, voids, and matrix observed.